Energy-absorbing effectiveness factor

Norman Jones

Accepted Manuscript

Title: Energy-absorbing effectiveness factor

Authors: Norman Jones

PII: S0734-743X(09)00026-8
DOI: 10.1016/j.ijimpeng.2009.01.008
Reference: IE 1747

To appear in: *International Journal of Impact Engineering*

Received Date: 15 October 2008
Revised Date: 30 January 2009
Accepted Date: 30 January 2009

Please cite this article as: Jones N. Energy-absorbing effectiveness factor, International Journal of Impact Engineering (2009), doi: 10.1016/j.ijimpeng.2009.01.008

ENERGY-ABSORBING EFFECTIVENESS FACTOR

Norman Jones

Department of Engineering, University of Liverpool, Liverpool L69 3GH, UK
Fax: 0151 794 4848. e-mail: norman.jones@liv.ac.uk

ABSTRACT

A study is reported on the energy-absorbing effectiveness factor which was introduced recently. The factor is defined as the quotient of the total energy, which can be absorbed in a system, to the maximum energy up to failure in a normal tensile specimen, which is made from the same volume of material. This dimensionless parameter allows comparisons to be made of the effectiveness of various geometrical shapes and of energy-absorbers made from different materials. The influence of material properties and various geometrical parameters on the value of the dimensionless parameter has been examined for the static and dynamic axial crushing behaviour of thin-walled sections. The influence of foam fillings and the stiffening of circular and square tubes is examined.

It transpires that, according to the energy-absorbing effectiveness factor, an axially crushed circular tube is the most effective structural shape, and that multi-cellular cross-sections, and axial stiffening, increases the effectiveness of thin-walled sections. In these later two cases, the energy absorbed by the additional material in a tensile test is included in the denominator of the energy-absorbing effectiveness factor. The influence of foam filling was found to increase the energy-absorbing effectiveness factor even though the additional energy absorbed by the foam is retained in the denominator. It was also noted that a circular tube, crushed axially either statically or dynamically, and made from an aluminium alloy, had a larger energy-absorbing effectiveness factor than a similar one made from a stainless steel, because the steel had a larger rupture strain which was not required during the deformation of the particular geometry examined.

KEY WORDS: energy-absorbing effectiveness factor, impact, tubes, top-hat, double-hat, circular, square, hexagonal, multi-cell, stiffened, foam-filled.

NOTATION

q	Cowper-Symonds exponent (equation ((8))
A	cross-sectional area of a thin-walled section
A_f	area of foam filling
C	side dimension of a square tube
D	Cowper-Symonds constant (equation (8)); mean diameter of a circular cylindrical shell
E_f	energy absorbed by foam filling
G	mass of striker
H	wall thickness of a thin-walled section
L	axial length
P	axial force
P_m	mean axial force
R	mean radius of a circular tube
T	depth of a stiffener
V	axial velocity; volume of material
V_o	initial impact velocity
δ	axial displacement
δ_e	dimensionless effective crushing distance = δ_f/L
δ_f	final axial displacement; bottoming-out displacement
ε	engineering strain
ε_r	rupture strain
$\dot{\varepsilon}$	strain rate
ρ_f	density of foam
σ	stress
σ_a	average stress
σ_y	static yield stress
σ_o, σ_o'	static and dynamic characteristic stresses
σ_u	ultimate tensile stress
ψ	static energy-absorbing effectiveness factor
ψ'	dynamic energy-absorbing effectiveness factor

1. INTRODUCTION

Extensive studies have been reported on the behaviour of systems which absorb external energy through the irreversible inelastic response of a material [1–4, etc.]. These dedicated energy absorbers are employed in many practical applications, but, in severe accidents, the actual structural member (e.g., a car framework) could be designed to deform in a specified manner and absorb additional dynamic energy. It turns out that a significant proportion of the studies undertaken have

been reported for mild steel tubes having various cross-sectional shapes and struck axially by rigid masses travelling with relatively low velocities up to about 10-15 m/s [5-7]. These energy absorbers are efficient, reliable, relatively inexpensive and are readily available in many structural geometries.

In more recent years, investigators have examined the advantages of using other materials, such as aluminium alloys [8] and high-strength steels [9,10]. However, any comparisons between the characteristics of energy absorbers, which are made from different materials, are difficult because of many factors, including the variety of deformation modes, some of which are symmetric, but many of which are not. The lack of experimental data on the strain rate sensitive properties and failure strains of the materials also cloud the comparisons. For example, some of the higher strength materials indicate a clear advantage over mild steel when loaded statically, but, in the dynamic range, the material strain rate sensitive strengthening of the high strength steels is less significant than for mild steel, and the failure strains are sometimes smaller as well, so that any advantage observed for static loads might be lost in the dynamic range. The response of several tube geometries made from high-strength steels have been studied experimentally in Reference [10] and the advantage of using these materials instead of mild steel has not been as great as anticipated.

Many parameters have been introduced by authors to assess the energy-absorbing characteristics and efficiencies of a wide range of structural members subjected to static and dynamic crushing loads [1,4]. These dimensionless parameters express the characteristics of energy absorbers in terms of their mass, volume, cost and other important properties. However, these studies are conducted usually in terms of one particular material or for one specified structural geometry. A designer, on the other hand, requires information on the choice of a material and the selection of a structural geometry which will lead to a design of the most efficient energy absorber.

A recent study has reported on the static and dynamic axial crushing behaviour of thin-walled cylindrical shells made from aluminium alloy, stainless steel and mild steel [11]. In order to assist in the comparison of the efficiencies of tubes made from different materials, an energy-absorbing effectiveness factor was introduced and defined as

$$\psi = \frac{\text{total elastic and plastic strain energy absorbed by a structural member}}{\text{energy absorbed in the same volume of material up to failure in tension}}. \qquad (1)$$

This paper discusses several forms of this dimensionless parameter, and explores its use to guide a designer in selecting a material and in choosing a structural geometry. The next section examines various forms of equation (1), while the following section uses it to explore the influence of different materials on the effectiveness of energy absorbers. Section 4 studies the influence of the structural geometry on their effectiveness according to equation (1). Sections 5 and 6 respectively examine the influence of stiffeners and internal foam filling on the effectiveness of energy absorbers. The paper concludes with a discussion and conclusions in sections 7 and 8, respectively.

2. ENERGY-ABSORBING EFFECTIVENESS FACTOR

Equation (1) might be written in the form

$$\psi = \frac{\int_0^{\delta_f} P d\delta}{V \int_0^{\varepsilon_f} \sigma d\varepsilon}, \qquad (2)$$

where P is the axial crushing force and δ is the corresponding axial crushing displacement which has a final value δ_f. The integral in the denominator of equation (2) is the energy absorbed in the same volume of material, V, up to rupture in a uniaxial tensile test specimen which is made from the same

material. A dynamic energy-absorbing effectiveness factor, ψ', is also defined, in [11], for energy-absorbing structural systems subjected to dynamic loads.

Several simpler forms of equation (2) are developed, in Reference [12], for the static and impact axial loading of energy-absorbing systems made from thin-walled sections. Clearly, if the relationships implicit in the numerator and denominator of equation (2) are known, then ψ can be determined. On the other hand, in the case of static loadings, the integral in the numerator usually can be calculated from the product of the mean axial crushing force, P_m, for progressive buckling of an energy-absorbing system and the final axial displacement, δ_f, both of which are often recorded in experimental studies. The numerator is replaced in the impact loading case by the initial kinetic energy, $GV_o^2/2$, and the additional potential energy acquired by the striking mass, G, during the crushing event (i.e. the total potential energy lost by the striking mass during the entire process until it reaches its final position).

In most experimental studies, only the static yield (σ_y) and ultimate tensile (σ_u) stresses are reported for the materials, sometimes together with the uniaxial tensile engineering rupture strain (ε_r). These values can be used to estimate the static and dynamic flow stresses σ_o and σ_o'. Thus, it might be assumed that

$$\psi = \frac{P_m \delta_f}{\sigma_o A L \varepsilon_r}, \tag{3}$$

and

$$\psi' = \frac{GV_o^2/2 + G\,g\,\delta_f}{\sigma_o' A L \varepsilon_r}, \tag{4}$$

for the static and impact cases, respectively, where A is the cross-sectional area and L is the initial axial length of an energy absorber. If the material strain rate sensitivity effects are neglected, i.e., $\sigma_o^{'}$ is taken as the static flow stress σ_o, and the additional potential energy of the mass due to the axial crushing of the energy absorber is neglected compared with the initial kinetic energy, then equation (4) becomes

$$\psi' = \frac{GV_o^2}{2\sigma_o AL\varepsilon_r} , \tag{5}$$

where the flow stress in equations (3) and (5) could be taken as $(\sigma_y + \sigma_u)/2$ to approximate the influence of material strain hardening effects in the corresponding integral in equation (2) when sufficient information on the material characteristics is available.

In most impact loading experiments, the actual crushing distance of an energy absorber might be smaller than the associated bottoming-out displacement [4]. In other words, the actual crushing displacement, δ_f, might be smaller than the effective crushing distance, δ_e. However, the effective crushing distance ratio $\delta_e / L \cong 3/4$ is a reasonable engineering approximation [12] so that the length L of an energy absorber in equation (5) is replaced by $4\delta_f / 3$ to reflect the axial length of an energy absorber which actually participates in absorbing the initial impact energy. Thus, equation (5) becomes

$$\psi' = \frac{3GV_o^2}{8\sigma_o A\delta_f \varepsilon_r} . \tag{6}$$

Similarly, equation (3) for static loading becomes

$$\psi = \frac{3P_m}{4A\sigma_o\varepsilon_r} . \tag{7}$$

3. INFLUENCE OF MATERIAL PROPERTIES

The original purpose of equation (1) was to allow a rational comparison to be made between the effectiveness of a particular design of an energy-absorber when made from different materials. The introduction of this dimensionless parameter in [11] revealed that the static axial loading of thin-walled aluminium alloy circular cylindrical shells was more effective than similar shells made from either mild steel or stainless steel, even though they absorbed significantly more energy per unit volume of the material. This factor was also higher for the axial impact loading of aluminium alloy circular cylindrical shells. The effectiveness is greatest when most of the available energy in the material is absorbed by an energy-absorbing device. It transpired that a uniaxial engineering rupture strain of 8.9% for an aluminium alloy material is sufficient for the dynamic axial crushing of the cylindrical shells studied in Reference [11]. The much larger engineering rupture strains of 33.4% and 59.3% for the mild steel and the stainless steel, respectively, are not reached during the crushing response of the cylindrical shells, which leads to an unused capacity of the material in energy-absorbing devices having the same geometry and loading.

The dynamic energy-absorbing effectiveness factors (equation (6) with $\sigma_o = (\sigma_y + \sigma_u)/2$) for the circular tube results reported in Reference [11], which are obtained using a common test rig with the same values of G and V_o, are plotted in Figure 1 with respect to the mean flow stress σ_o for three different materials (aluminium alloy, mild steel and stainless steel). This Figure shows a clear reduction in ψ' with an increase of σ_o, as indicated by equation (6) when taking all the parameters to remain constant except σ_o, though in Figure 1, there are differences in the values of A, δ_f and ε_r for the three shells.

Xue et al [13] have examined square tubes made from mild steel(σ_o= 372 MPa) and stainless steel (AISI 304, σ_o= 604 MPa) and the energy-absorbing effectiveness factors from equation(6) show that ψ' = 0.54 for the stainless steel test specimen H7, while ψ' = 2.95 for the mild steel specimen S4. These two square tube results in Figure 2 reveal a trend which is consistent with that in Figure 1 for circular tubes. Several other studies [14-16] on square tubes with G < 100 kg, which are reported in Table 2 of Reference [12], are also presented in Figure 2, but the trend of ψ' reducing with an increase in σ_o, observed in Figure 1, is far less clear because of the scatter in the results, as discussed in the next paragraph. However, the data in Figure 2 are replotted with respect to $\sigma_o\varepsilon_r$ in Figure 3 and a more consistent trend in the results is observed. The experimental results on square tubes, which are reported in References [5, 10, 17], as well as the data from Table 2 of Reference [12] with G > 100kg, are also plotted in Figure 3.

The scatter of the results in Figures 2 and 3, which were obtained from several laboratories, might arise from various factors. For example, the specimen dimensions differ between experimental studies, as well as the impact velocities and the striking masses. The experimental loading devices include drop hammer rigs, Hopkinson pressure bar arrangements and servo-hydraulic machines. Some specimens are manufactured using spot welds, while others are welded and several are pre-triggered. The proportion of the initial axial length, which is crushed during a test, varies from specimen to specimen leading to a different contribution of the initial peak load to the mean force, P_m.

Wu and Jiang [18] have studied aluminium alloy 5052-H38 thin-walled honeycomb sections (H = 0.0254 mm, σ_o = 272.5 MPa) and equation (6) reveals that ψ' ranged from 3.29 to 4.54 for axial impact velocities up to 26.4 m/s. Additional tests were reported in Reference [18] on

aluminium alloy 5056-H38 honeycombs having σ_o = 380 MPa and with ψ' lying between 1.59 and 1.81 for impact velocities up to 28.1 m/s. Furthermore, the results from Table 5 of Reference [12], which are calculated from the data reported in References [9, 19, 20], predict values for ψ' up to 1.02 for honeycomb specimens made from a TRIP 600 steel with σ_o = 558.5 MPa . The trend for these honeycomb sections is shown in Figure 4 and is consistent with that shown in Figure 1 for circular sections.

The impact behaviour of most energy-absorbing systems is analysed using the simplification of quasi-static behaviour, for which the deformation response is similar to the static behaviour [21]. Thus, equation (6) with the static flow stress, σ_o, was used for the results in Figures 1 to 4. However, the strain rate sensitivity of some materials might be important even for relatively low impact velocities when the behaviour can be taken as quasi-static. Unfortunately, most of the studies reported on the behaviour of energy-absorbing systems under impact loadings have not reported the dynamic properties of the associated materials. In this circumstance, the dynamic flow stress, σ_o', could be estimated using the Cowper Symonds constitutive equation [4]

$$\frac{\sigma_o'}{\sigma_o} = 1 + \left(\frac{\dot{\varepsilon}}{D}\right)^{\frac{1}{q}}, \qquad (8)$$

where D and q are material constants and σ_o' could be used to replace the static flow stress σ_o in the denominator of equation (6), which was used for the results reported in Figures 1 to 4. Equation (8) was used in Reference [12] to estimate the influence of material strain rate sensitivity on the dynamic axial crushing behaviour of thin-walled tubes with circular cross-sections. The estimate in References [4, 12] of $\dot{\varepsilon} = V_o/4R$ gives $\dot{\varepsilon}$ = 136, 133 and 135 $\sec^{-1}$ for the stainless steel, aluminium alloy and mild steel cylindrical shells in Figure 1 having R = 24.37, 24.88 and

24.57 mm, respectively, and V_o = 13.28 m/s. These strain rates are within the range of the dynamic tensile test values reported in Reference [11]. Now, using the values of D and q given in Table 1(b) of [11] for the dynamic yield stresses, equation (8) predicts enhancement factors of 1.33, 1.12 and 2.03 for the dynamic flow stresses of the stainless steel, aluminium alloy and mild steel tubes studied in Reference [11], respectively. Equation (8) with this approximation for $\dot{\varepsilon}$ gives fairly crude estimates of the material strain rate sensitive characteristics since the actual strain rate varies both spatially and temporally during the deformation of a tube and is zero when motion ceases. Moreover, the enhancement of the ultimate tensile stress usually is smaller than that for the yield stress given by equation (8) [22], as illustrated by the much larger values of D in Table 1(b), in Reference [11], for the three materials examined in Reference [12] and Figure 1 here. Thus, the actual enhancement factors due to material strain rate effects are likely to be smaller than those estimated above. Moreover, the strain rate sensitivity of a material according to equation (8) is a highly non-linear phenomenon because the values of q are larger than 1 (typically 4 to 10) so that fairly crude estimates of the strain rate can lead to reasonable engineering estimates of the corresponding dynamic flow stress. In fact, it is shown, in Reference [12], that the above consideration of the dynamic flow stress does not change the order of merit of the circular tubes made from the three materials. Nevertheless, it would be worthwhile to obtain the dynamic material properties of the materials used in any future studies of energy-absorbing systems since this phenomenon could change the relative values of the energy-absorbing effectiveness factors.

4. INFLUENCE OF CROSS-SECTION GEOMETRY

Reference [12] has explored the energy-absorbing effectiveness factors for discriminating between thin-walled tubes having different cross-sectional geometries under static and dynamic

($V_o \leq 20$ m/s) axial crushing forces. The most striking observation for mild steel specimens is that a circular section is the most effective and a top-hat section the least effective, with the double-hat section marginally better, as shown in Figure 5. Unfortunately, a paucity of published data does not allow the comparison of different section geometries in figures similar to Figure 5 for other materials. Furthermore, it appears that no suitable data are available for hexagonal sections made from mild steel and which could be added to Figure 5. Nevertheless, it might be anticipated that the behaviour of hexagonal sections would lie between the square and circular sections in Figure 5. Indeed, although not strictly comparable, it is observed that the values of ψ' in Figure 4, for aluminium alloy 5052-H38 honeycomb sections having $\sigma_o = 272.5$ MPa, are larger than those in Figure 2 for square sections made from an aluminium alloy 6060 T6 having $\sigma_o = 198$ MPa and $\sigma_o = 203$ MPa. Incidentally, the honeycomb sections in Reference [18] are constructed with 10 to 23 cells, which would, possibly, provide a stiffer structure than a single hexagonal section and lead to an unknown enhancement of ψ'.

Tables 3 and 5 in Reference [12] report some data for top-hat and hexagonal sections made from a TRIP 600 steel ($\sigma_o = 558.5$ MPa) [9, 19, 20]. The values of ψ and ψ' for the hexagonal sections have average values of 0.88 and 0.93, respectively, while the corresponding values for the top-hat sections are 0.44 and 0.65. This behaviour follows the trend in Figure 5 for mild steel sections. Nevertheless, the results for a high strength steel (HSLA) with $\sigma_o = 374.5$ MPa in Tables 2 and 3 of Reference [12] for square tubes and top-hat sections, show that ψ are similar for both geometries, while ψ' are also similar but are somewhat larger.

It is evident that there are many test, material and geometrical parameters which could influence the comparisons. For example, it is indicated in Figure 6 that ψ' tends to increase with

the cross-sectional area, A, of aluminium alloy 6061 tubes having a rectangular cross-section and subjected to dynamic axial loads [23]. On the other hand, equation (6) suggests that ψ' should decrease with an increase in A when all other parameters remain unchanged. Nevertheless, the axial crushing displacement, δ_f, would likely decrease with an increase in A for the same impact energy. Thus, it might be anticipated that ψ' would not change since the product $A\delta_f$, which is related to the volume of material actively absorbing the initial impact energy, might remain essentially constant. However, it should be noted that inertia effects cause the value of δ_f to decrease as the impact velocity is increased (see Figure 5 in Reference [27] for a cylindrical shells and Figure 13 of [28] for square tubes). This phenomenon would give rise to a decrease in the product $A\delta_f$ and an increase in ψ' according to equation (6), but does not influence the particular results in Figure 6 since the initial impact velocity is constant. The experimental results reported in Reference [23] for dynamically crushed aluminium alloy 6061 circular tubes do not reveal a clear variation of ψ' with A. Moreover, the statically crushed empty square steel tubes in Reference [29] have values of ψ which decrease with an increase in A.

A reduction in ψ' occurs with an increase of the diameter-to-thickness ratio, 2R/H, for the dynamically crushed aluminium alloy circular tubes studied in Reference [23], as shown in Figure 7(a). A somewhat similar trend with respect to the mean values of the C/H ratio is observed in Figure 7(b) for the tubes having rectangular and square cross-sections and reported in Reference [23]. Figure 8(a) indicates that there is a tendency of ψ' to increase with an increase in the axial impact velocity, V_o, for both square and circular aluminium alloy tubes. This tendency is also observed in Figure 8(b) for honeycomb, top-hat and square sections which are made from several materials. It should be noted here that the initial dynamic peak force, in circular and square tubes

impacted axially, is a function of the initial impact velocity,V_o, due to inertia effects (see equations (26-27) in [31] for cylindrical shells and Figure 14 in [28] for square tubes). Equation (2) for dynamic loadings can be written in a form similar to equation (7) when the material is strain rate insensitive and P_m corresponds to the mean dynamic crushing force. Thus, it is likely that ψ' would increase with V_o, as shown in Figure 8(a,b).

5. INLUENCE OF STIFFENERS

The energy-absorbing effectiveness factor, which is defined by equation (1), can be used to explore the influence of stiffeners on the efficiency of thin-walled sections subjected to axial crushing forces. Reference [32] reports on an experimental programme undertaken on mild steel cylindrical shells of thickness H and a mean diameter D, which are stiffened with N longitudinal stiffeners having rectangular cross-sections of radial depth T and thickness H, subjected to static and dynamic axial crushing forces up to initial velocities of 11.7 m/s. For comparison purposes, the behaviour of some unstiffened tubes made from the same mild steel, are also reported in Reference [32]. The values of ψ and ψ' for the unstiffened tubes (N = 0) and those with either four internal or four external stiffeners (N = 4) are presented in Figure 9. It is evident that the influence of stiffeners always leads to significantly larger values of the dynamic energy-absorbing effectiveness factor ψ' than that observed for static loadings, ψ. Moreover, it is evident that the greatest improvement occurs for small stiffeners having T/D up to about 0.10 and that there is no further gain for larger values of T/D. Although there is some scatter in the results in Figure 9, the trend for impact loadings suggests that the external stiffeners are more effective than similar

internal ones, while the opposite case occurs for static loadings. It is interesting to note that the theoretical study on the dynamic plastic buckling of axially stiffened cylindrical shells, which is reported in Reference [33], found that it is most efficient to place the optimum stiffeners on the outside surface of a cylindrical tube.

Equation (6) shows that ψ' is proportional to $1/A\delta_f$ when the remaining parameters are treated as a constant. In other words,

$$\frac{\psi'_1}{\psi'_2} = \frac{A_2\delta_{f2}}{A_1\delta_{f1}} \quad . \tag{9}$$

Thus, comparing specimen 5IF49 having four internal stiffeners (T/D = 0.12) with the unstiffened case (specimen 5NF00) having the same values of G, V_o, σ_o and ε_r [32] gives ψ'_1/ψ'_2 = 1.33. Similarly, comparing specimen 5EF49 with four external stiffeners having T/D = 0.12 with specimen 5NF00 gives ψ'_1/ψ'_2 = 1.58. These calculations indicate the enhancement in ψ' to be gained by circular cylindrical shells having four longitudinal stiffeners with T/D = 0.12 and struck by a mass travelling at an axial impact velocity of 11.7 m/s.

Experimental data are also reported in Reference [32] for the same mild steel circular shells but stiffened with either 8 or 12 longitudinal stiffeners. However, in many cases, this additional stiffening causes overall or global buckling modes to develop rather than progressive buckling. For progressive buckling, the velocity-time history at the proximal end of a tube in Reference [32] decreases linearly to give a constant acceleration and, therefore, a constant mean crushing force, P_m. It is evident from the results reported in Reference [32] that the shape of the velocity-time history curves at the proximal ends of tubes stiffened with 8 or 12 longitudinal stiffeners is concave giving rise to unstable results.

Some static and dynamic axial crushing tests are reported, in Reference [34], for longitudinally stiffened and unstiffened mild steel square tubes. The tubes have a side length C = 49.2 mm, thickness H = 1.63 mm and the stiffeners have rectangular cross-sections of depth T and thickness H. The energy-absorbing effectiveness factors ψ and ψ' are calculated using equations (7) and (6), and are presented in Figure 10 for both internally and externally stiffened square tubes having N = 4. It is evident that the factors for the impact cases are only marginally larger than the corresponding static values, unlike the stiffened circular tube results reported in Figure 9. Nevertheless, the stiffening does cause ψ and ψ' to increase with an increase in the size of a longitudinal stiffener. The only exception to the above observations are the results in Figure 10 for the four largest internal stiffeners having T/C = 0.38. It is reported, in Reference [34], that there was evidence of interference between the internal stringers having T/C = 0.38 during the buckling process. This phenomenon would likely lead to an increase in the axial resistance of a tube and give rise to a smaller than expected axial deformation and, therefore, a higher value for ψ', as shown in Figure 10. It is noted here that Paik et al [35] also observed this phenomenon for square tubes stiffened externally with the deepest stiffeners.

Equation (9) is a general expression, which was used earlier for stiffened circular cylindrical tubes, but it is equally valid for longitudinally stiffened square tubes. A comparison of test specimen 11B with four external stiffeners having T/C = 0.12 and the unstiffened test specimen 5B, both loaded at 11.7 m/s, gives $\psi'_1 / \psi'_2 = 1.32$. Thus, the four external longitudinal stiffeners are responsible for a 32 per cent enhancement of the energy-absorbing effectiveness factor.

The experimental data in Figures 9 and 10 for the axial crushing of mild steel circular and square shells with four longitudinal stiffeners reveal the potential advantages of longitudinal stiffening. In fact, it is evident from the results in Figure 9 for external stiffeners with T/D = 0.12

that ψ' is larger than the unstiffened circular tube results in Figure 5. Moreover, ψ' for the square tubes with stiffeners having T/D =0.12 in Figure 10 are between the unstiffened circular and square tubes in Figure 5.

Reference [34] also presents some experimental data on square tubes having 8 and 12 longitudinal stiffeners, but, generally speaking, the deformed profiles are not the classical progressive buckling forms which are associated, usually, with efficient energy-absorbing systems.

The experimental results reported in Figures 9 and 10 have been calculated by assuming that the dimensionless effective crushing distance is $\delta_e/L = 0.75$ for both static and impact loadings. The actual value is a function of the shell dimensions, as illustrated by equation (9.26) in Reference [4], but this expression, and others, have been developed for unstiffened cylindrical shells. Paik et al [35, 36] have recognised the important influence that longitudinal stiffeners have on this phenomenon. Paik smears the stiffeners to give an equivalent shell thickness and presents an empirical equation for the dimensionless effective crushing distance, which varies with the geometry of a statically loaded square tube. This phenomenon can give rise to smaller values of δ_e/L (see Figure 16 of Paik et al [35]), which would cause a reduction in ψ and ψ' for the experimental results presented in Figures 9 and 10. However, although the actual values of ψ and ψ' would decrease for a given value of T/D or T/C, in some cases, the relative ratio of two values would remain unchanged when assuming that the empirical relation for the dimensionless effective displacement, which is obtained by Paik et al [35] for static loadings, remains valid for impact loadings of similar stiffened shells. For example, the calculations based on equation (9) would remain unchanged provided that they refer to the static and impact behaviour of shells having the same number and size of stiffeners and the same shell geometry. However, this phenomenon could give rise to different values of δ_e/L for stiffened and unstiffened tubes.

If the dimensionless effective crushing distance of 3/4 embodied in equation (7) for static loadings is replaced by the more general expression δ_e/L, then

$$\psi = \frac{P_m(\delta_e / L)}{A\sigma_o\varepsilon_r} \quad , \tag{10}$$

which indicates that ψ is proportional to $P_m\delta_e/A$ for shells having the same material properties σ_o and ε_r and axial length L. Thus,

$$\frac{\psi_1}{\psi_2} = \frac{P_{m1}\delta_{e1}A_2}{P_{m2}\delta_{e2}A_1}, \tag{11}$$

where the dimensionless effective crushing distances are presented in Table 2(sic) of Reference [35] for most of the experimental results recorded on square tubes loaded statically. Equation (11) gives $\psi_1/\psi_2 = 1.11$ for the statically loaded square tube LS-1 (N = 4, T/C = 0.2) when compared with its unstiffened counterpart (US-2). Similarly, $\psi_1/\psi_2 = 1.38$ for LS-2 (N = 4, T/C = 0.3) when compared with the corresponding unstiffened case (US-2). Thus, the static energy-absorbing effectiveness factor is increased by 11 per cent and 38 per cent for these two square tubes having N = 4 and T/C = 0.2 and 0.3, respectively. This increase is somewhat smaller than that for the static results reported in Figure 10, but it does, nevertheless, support the observation that longitudinal stiffeners in square tubes do increase the factor ψ. The values of ψ for the longitudinally stiffened square tubes studied in Reference [35] are given in Table 1. It is evident that ψ increases as the T/C value is increased for the external stiffeners.

Adachi et al [37] have reported some experimental results on the energy-absorbing characteristics of thin-walled cylindrical shells with transverse (circumferential) external ribs. The shells are subjected to axial loads at relatively low impact velocities produced by a mass dropped from heights up to 2 m. The energy-absorbing effectiveness factor can be calculated for this case

by smearing the circumferential stiffeners over the shell surface and using an equivalent shell thickness for calculating the area A in equation (6). The uniaxial rupture strains for the aluminium alloy 6063 material used to manufacture the tube specimens are not reported in Reference [37]. Thus, an engineering rupture strain, $\varepsilon_r = 0.089$, was taken from Reference [11] for aluminium alloy 6063 T6. If $E_a = GV_o^2/2$ and δ_f are obtained from graphs in Reference [37], then it is found that equation (6) gives $\psi' = 0.90$, 0.92, 0.93 and 0.94 for unstiffened (RO-SA-1), stiffened with circumferential ribs (average of R2-SA-1, 2, 3, 5), stiffened with four circumferential ribs (R4-SA-1, 2) and stiffened with six circumferential ribs (R6-SA-1, 2), respectively. It appears that there is no practical improvement in the value of ψ' when using circumferential stiffeners and, therefore, they have no advantage, at least as far as the energy-absorbing effectiveness factor is concerned.

Equation (6) assumes that the dimensionless effective crushing displacement is 0.75 for all specimens. However, even if the actual value is different and is related to the number of circumferential stiffeners, for example, the relative difference would still likely be insufficient to recommend the placing of circumferential stiffeners on the outside surface of axially impacted cylindrical shells, at least from the perspective of the energy-absorbing effectiveness factor.

References [38-41] have studied the relative merits of several cross-sectional shapes subjected to static axial crushing loads, but since these references contain no new experimental data, this work is returned to in section 7.

6. INFLUENCE OF FOAM FILLINGS.

If a tube is filled with a foam then the energy which could be absorbed in crushing this foam must be retained in the calculation for the energy-absorbing effectiveness factor. Strictly speaking, the energy that could be absorbed by the foam until the associated locking strain is reached should be included in the denominator of equation (6). However, it is evident from the data in Reference

[42] that the locking strain of that particular aluminium foam is much larger than the rupture strain of the surrounding aluminium alloy shell. Thus, to simplify an analysis, it is assumed that the maximum strain reached in the foam is equal to the uniaxial rupture strain of the shell material. Thus, the energy absorbed in the foam during a simple compression test is taken as

$$E_f = \sigma_f A_f \delta_f (4/3) \varepsilon_r \ , \tag{12}$$

where σ_f is the plateau crushing stress of the foam, A_f is the cross-sectional area of the foam infilling, δ_f is the final crushing displacement of the composite and the dimensionless effective crushing displacement is taken as 3/4. Equation (12) must be added to the denominator of equation (6) to give

$$\psi' = \frac{3GV_o^2}{8\delta_f \varepsilon_r (\sigma_o A_s + \sigma_f A_f)}, \tag{13}$$

where σ_o is the mean flow stress of the metal shell and A_s is the cross-sectional area of the shell.

Figure 11 presents some results from Reference [42] for aluminium alloy 6060 square tubes filled with an aluminium foam having a density ρ_f and impacted axially. These results reveal that ψ', which is calculated for a square tube using equation (13), increases significantly with an increase in the foam density ρ_f, or increase in the foam strength, and also increases with the mean flow stress, σ_o, of the tube material for a given value of ρ_f. Hanssen et al [43] have studied circular tubes made from aluminium alloy 6060 T4 and filled with an aluminium foam and the energy-absorbing effectiveness factors according to equation (13) also increase significantly with an increase in the foam density, or foam strength, as shown in Figure 12. In other words, the energy-absorbing effectiveness factors in Figures 11 and 12 reveal that it is advantageous to fill the thin-walled aluminium alloy square and circular tubes in References [42] and [43] with an aluminium foam.

7. DISCUSSION

Several authors [e.g. 38-41] have used numerical finite-element schemes to compare the energy-absorbing capacities of tubes having various cross-sections and subjected to axial crushing loads. However, most of these studies have examined the behaviour due to static loadings, although one recent numerical study has considered square and multi-cell designs for axial impact loadings at 10 m/s [41]. An optimal design was sought by maximising the energy absorption efficiency and minimising the peak axial crushing force. It transpires that the larger the number of cells, the higher is the maximum specific energy absorption, but no regularity was observed for the peak crushing force objective. This article [41] is focussed largely on the different possible optimisation formulations and there is insufficient information presented to permit the calculation of the dynamic energy-absorbing effectiveness factor from equation (6).

Chen and Wierzbicki [38] have studied the energy-absorption characteristics of the single-cell and multi-cell thin-walled structures shown in Figure 13 and explored the advantages of foam-filling when subjected to static axial loads. It was observed that some rigid plastic theoretical predictions gave good agreement with the corresponding numerical predictions. The dimensionless effective crushing displacement is taken as 0.73, which agrees with the theoretical prediction and the numerical calculations. The theoretical expressions in Reference [38] are now used to calculate the static energy-absorbing effectiveness factor.

Chen and Wierzbicki [38] found that the mean static crushing force for a multi-cell section is

$$P_m = 2\sigma_o H(\pi NA)^{1/2} / 3 , \qquad (14)$$

where A is the total cross-sectional area, N is the number of contributing flanges [38] and when assuming that $\delta_e/L = 0.75$. For the double-cell section in Figure 13(b), N = 14 and A = 5CH, so that equation (14) gives

$$P'_m = 9.89\sigma_o C^{1/2} H^{3/2} \ . \qquad (15)$$

Similarly,

$$P''_m = 12.94\sigma_o C^{1/2} H^{3/2} \qquad (16)$$

for the triple-cell section in Figure 13 (c) with N = 20 and A = 6CH. Now, equation (7) might be used to obtain the static energy-absorbing effectiveness factors for these sections since $\delta_e/L = 0.75$ was used in deriving equation (14). The good agreement that Chen and Wierzbicki [38] observed between the above theoretical predictions and the corresponding numerical calculations was obtained for aluminium alloy 6061 T4 with σ_y =110.3 MPa, σ_u = 213 MPa and ε_r =0.19. This gives a mean flow stress σ_o = 161.7 MPa (equation (17) in Reference [38] was used to calculate the average stress as σ_o =177.5 MPa and used in their calculations). Equations (7) and (15) predict that $\psi = 7.808(H/C)^{1/2}$ so that the thicker tubes are more effective and $\psi > 1$ when C/H < 61. Chen and Wierzbicki [38] studied double-cell sections with 21 < C/H < 80. Similarly, equations (7) and (16) for a triple-cell section gave $\psi = 8.513(H/C)^{1/2}$. In this case, $\psi > 1$ provided C/H < 72.5. It is evident that increasing the cross-sectional area from a double-cell to a triple-cell section gives an improvement in the static energy-absorbing effectiveness factor of 8.513/7.808, or about 9 per cent. Thus, it is advantageous to increase the number of cells (at least two to three) from the perspective of the static energy-absorbing effectiveness factor. In fact, the results in Table 2 show that ψ increases as the number of cells is increased from a single cell square tube.

Chen and Wierzbicki [38] have explored the effect of infilling the sections with lightweight cellular materials, such as an aluminium foam. The static crushing resistance and energy absorption of the thin-walled sections were increased through the direct compressive strength of the foam and by the foam filler acting as a foundation to the enclosing section wall. The direct

compressive strength should be considered in calculations of the energy-absorbing effectiveness factor, as in equation (13) for dynamic loadings. However, the additional enhancement due to the interaction effect between the foam filler and the shell wall should not be retained in the denominator of equation (13), or its static equivalent expression, because that effect would not arise in a uniaxial compression test on the foam. This effect, arises through the interaction of a foam with the thin-walled section, and would appear in the expression for the energy absorbed in the numerator. Santosa et al [44] found from comparisons between some particular tests on foam-filled square sections and numerical calculations that the interaction effect was about 80 per cent of the uniaxial crushing strength of the foam. Reference [38] reports that this interaction effect was even more significant at 140 per cent and 180 per cent for the respective foam-filled double-cell and triple-cell sections having the geometries shown in Figure 13. Thus, the values of the static energy-absorbing effectiveness factors for these sections would be even larger than those without a foam-filling, as indicated in Table 2. Incidentally, it was observed from the numerical calculations in Reference [38] that $\delta_e/L \approx 0.73$ for the foam-filled tubes which is similar to the value for the corresponding empty ones. Some additional comments on the behaviour of foam-filled tubes are reported in Reference [45]. Thus, from the viewpoint of the static energy-absorbing effectiveness factor, it is advantageous to have three cells rather than two and it is a further advantage to have a foam-filling, as shown in Table 2; this later observation is consistent with that shown in Figures 11 and 12 for square and circular tubes, respectively.

Zhang and Suzuki [39] have used a finite-element numerical scheme to study the static axial crushing behaviour of the stiffened square tubes tested by Paik et al [35] and discussed in Section 5. The authors improved on the expression for the equivalent plate thickness used in References [34] and [36], etc., by introducing factors which recognise, more accurately, the contribution of the

transverse stiffeners. The resulting expression now discriminates between the contributions of the transverse and longitudinal stiffeners in the calculation of the equivalent thickness. However, the static energy-absorbing effectiveness factors for the experimental data on square tubes with longitudinal stiffeners have been discussed already in Section 5 and the broad observations remain unchanged.

Zhang and Cheng [40] have also used a finite-element method to compare the static behaviour of multi-cell columns with foam-filled square columns. The authors extended Chen and Wierzbicki's [38] method to predict a mean crushing force for any number of cells in a multi-cell section. In this study, they compared the behaviour of foam-filled square tubes with empty multi-cell tubes having the same total weight. It was observed that the energy-absorbing efficiency of an empty multi-cell section was higher than that for a foam-filled square tube. Unfortunately, insufficient information is reported in Reference [40] to enable a calculation of the static energy-absorbing effectiveness factor to be made and, thus, to obtain the relative efficiencies according to the static equivalent of equation (13). However, there is sufficient information in Reference [38] to construct Table 2 which compares the static energy-absorbing effectiveness factors for empty and foam-filled square, double-cell and triple-cell sections having the shapes illustrated in Figure 13. It is evident, for these particular parameters, that the double-cell and triple-cell cases have static values higher than that for a square tube and that a foam infilling provides a further significant improvement. Thus, these conclusions are different to those in Reference [40], though, as mentioned above, the ψ values could not be calculated from the numerical results they presented in the article. Nevertheless, it demonstrates that this class of problems contains a large number of parameters and, therefore, further study is required, particularly experimental testing, in order to

obtain the basic data which is necessary to calibrate the various numerical schemes and to test the theoretical developments.

As mentioned in Section 3, this article has focussed on the quasi-static behaviour of energy-absorbing systems, although the dynamic energy-absorbing effectiveness factor, defined by equation (1), does take inertia effects into account. The quantities in equation (1), such as the final axial displacement and the dynamic crushing force, could be obtained from the results of experimental impact tests or from numerical schemes which retain inertia effects. It should be noted that relatively high impact velocities are associated with the collision of high speed trains, for example, for which inertia effects could be important, as well as the influence of material strain rate sensitivity considered already in Section 3.

Broadly speaking, transverse or lateral inertia effects in axially crushed tubes are largely responsible for restricting development of the deformation profile, while the influence of axial inertia gives rise to elastic and plastic stress wave propagation in the longitudinal direction of a tube. Stress wave propagation has been studied for the axial impact behaviour of elastic-plastic circular cylindrical shells [46] and square tubes [28]. Transverse inertia can restrict the transverse, lateral or radial deformations of a tube, so that its initial shape remains straight for a longer period of time, thereby allowing it to absorb a significant amount of the initial impact energy in axial compression. This form of energy absorption is neglected in a theoretical quasi-static analysis and in design calculations [4, 21]. Furthermore, axial inertia can give rise to significant changes in the deformed profile of a tube due to the propagation, reflection and interaction of elastic and plastic stress waves [28, 46]. In these circumstances, a quasi-static analysis would be misleading. Nevertheless, the energy-absorbing effectiveness factor can still be used whether or not axial and

transverse inertia effects are important, provided the information for the integrals in the numerator and denominator of equation (1) is available.

If a tube is too long, then an overall or global buckling (Euler-type instability) might develop instead of the efficient energy-absorbing mechanism of progressive buckling. Again the onset of an instability might be delayed in the dynamic case because the transverse inertial resistance maintains a tube in its original straight shape for a finite time while some of the initial impact energy is absorbed during the axial squashing of a tube [47]. The energy remaining in the system, after the initial impact velocity has decreased sufficiently to reduce the transverse inertial resistance, might be insufficient to cause an overall instability so that a progressive buckling response ensues [47, 48]. The dynamic energy-absorbing effectiveness factor given by the dynamic counterpart of equation (1) can still be used, but the values would be small and reveal how inefficient this particular deformation mode is for absorbing impact energy.

8. CONCLUSIONS

An energy-absorbing effectiveness factor, identified by equation (1), was introduced recently and used to study the effectiveness of thin-walled structural sections having various shapes and subjected to static and dynamic axial loadings. This dimensionless factor was also used to discriminate between the effectiveness of different materials and to examine the efficiency of foam fillings. It was observed, for example, that a circular shape is the most efficient geometry. Moreover, it was found that an aluminium alloy is more effective than a stainless steel for circular tubes, because the higher rupture strain of the steel leads to an inefficient use of the material, whereas the lower rupture strain of the aluminium alloy was sufficient for absorbing the static and dynamic energies. Multi-cell sections and the addition of axial stiffeners on thin-walled sections both have higher energy-absorbing effectiveness factors than single cells and unstiffened sections,

respectively. Nevertheless, it is important to assess whether or not such geometrical changes lead to significant changes in the crushing behaviour. For example, excessive axial stiffening might lead to an inefficient global instability of a thin-walled section rather than an efficient static or dynamic progressive buckling response.

The energy-absorbing effectiveness factor can be used by a designer to choose an efficient cross-sectional shape and to aid in the selection of an appropriate material for manufacture. This factor is one of many dimensionless parameters available to a designer, but it is the only one, to the author's knowledge, which relates the energy absorbed by an energy-absorber to the energy potential of the material which is used in its manufacture. The broad definition of the energy-absorbing effectiveness factor means that various effects, such as new materials, stiffeners, foam filling and new shapes, can be assessed in order to seek the degree of any enhancement over simpler systems.

ACKNOWLEDMENTS

The author is grateful to Mrs. J. Jones and Mrs. I. M. Arnot for their assistance with this manuscript.

REFERENCES

1. Ezra, A. A., Fay, R. J., An assessment of energy absorbing devices for prospective use in aircraft impact situations, Dynamic Response of Structures, Edited by G. Herrmann and N. Perrone, Pergamon Press, New York, 225-246, 1972

2. Johnson, W., Mamalis, A. G., Crashworthiness of vehicles, MEP Ltd, London, 1978

3. Johnson, W., Reid, S. R., Metallic energy dissipating systems, Applied Mechanics Reviews, Vol.31, 277-288, 1978 and Vol.39, 315-319, 1986

4. Jones, N., Structural Impact, Cambridge University Press, Cambridge, 1989 and 1997

5. Abramowicz, W., Jones, N., Dynamic progressive buckling of circular and square tubes , International Journal of Impact Engineering, Vol. 4, No. 4, 243-270, 1986.

6. White, M. D., Jones, N., A theoretical analysis for the dynamic axial crushing of top-hat and double-hat thin-walled sections, Proceedings, Institution of Mechanical Engineers, Vol. 213, Part D, 307-325, 1999.

7. Gupta, N. K., Abbas, H., On Analysis of Axisymmetric Crushing of Tubes and Frusta, Advances in Dynamics and Impact Mechanics, Ed., C.A.Brebbia, and G. N. Nurick, W I T Press, Southampton, U.K., and Boston, U. S., pp 23-54, 2003.

8. Langseth, M., Hopperstad, O. S., Berstad, T., Crashworthiness of aluminium extrusions: validation of numerical simulation, effect of mass ratio and impact velocity, Int. J. of Impact Engng , Vol. 22, No. 9-10, 829-854, 1999.

9. Peixinho, N., Jones, N., Pinho, A., Determination of Crash-Relevant Material Properties of Dual-Phase and Trip Steels, proc. 8th International Symposium on Plasticity and Impact Mechanics, IMPLAST 2003, Ed. N. K. Gupta, Phoenix Publishing House, New Delhi, pp 343-353, 2003.

10. Schneider, F. D., Jones, N., Impact of Thin-Walled High-Strength Steel Structural Sections, proc. Institution of Mechanical Engineers, Vol. 218, Part D, Journal of Automobile Engineering, 131-158, 2004.

11. Hsu, S.S., Jones, N., Quasi-Static and Dynamic Axial Crushing of Thin-Walled Circular Stainless Steel, Mild Steel and Aluminium Alloy Tubes, International Journal of Crashworthiness, Vol. 9, No. 2, 195-217, 2004.

12. Jones, N., Energy absorption effectiveness of thin-walled structures under static and dynamic axial crushing loads, Impact Loading of Lightweight Structures, M. Alves, and N. Jones (Editors), WIT Press, Southampton and Boston, WIT Transactions on Engineering Sciences Vol. 49, pp 273-287, 2005.

13. Xue, L., Lin, Z., Zhang, Y., Jiang, Z., Dynamic axial crushing of stainless steel and mild steel square tubes, Proceedings of International Crashworthiness Conference, Ed. E. C. Chirwa and D. Otte, ICrash 2000, Published by Automotive Engineering, The Bolton Institute, pp 518-534, 2000.

14. Abramowicz, W., Jones, N., Dynamic axial crushing of square tubes, International Journal of Impact Engineering, Vol. 2, No. 2, 179-208, 1984.

15. Langseth, M., Hopperstad, O. S., Static and Dynamic axial crushing of square thin-walled aluminium extrusions, International Journal of Impact Engineering, Vol. 18, No. 7/8, 949-968, 1996

16. Zhao, H., Abdennadher, S., Othman, R., An experimental study of square tube crushing under impact loading using a modified large scale SHPB, International Journal of Impact Engineering, Vol. 32, No. 7, 1174-1189, 2006.

17. Jensen, O., Langseth, M., Hopperstad, O. S., Experimental investigations on the behaviour of short to long square aluminium tubes subjected to axial loading, International Journal of Impact Engineering, Vol. 30, No. 8/9, 973-1003, 2004.

18. Wu, E., Jiang, W. S., Axial crush of metallic honeycombs, International Journal of Impact Engineering, Vol. 19, No. 5/6, 439-456, 1997.

19. Peixinho, N., Jones, N., Pinho, A., Experimental and numerical study in axial crushing of thin-walled sections made of high-strength steels, J. Physique IV France, Vol.110, 717-722, 2003

20. Peixinho, N. R. M., Study of visco-plasticity models for the provision of mechanical behaviour of high strength steels subjected to impact, Ph.D. Thesis, Universidade do Minho, Guimaraes, 2004

21. Jones, N., Quasi-static analysis of structural impact damage, Journal of Constructional Steel Research, Vol. 33, No. 3, 151-177, 1995.

22. Jones, N., Some Comments on the Modelling of Material Properties for Dynamic Structural Plasticity, International Conference on the Mechanical Properties of Materials at High Rates of Strain, Oxford. Ed. J. Harding, Institute of Physics Conference Series No. 102, pp 435-445, 1989.

23. Kim, D-K., Lee, S., Impact energy absorption of 6061 aluminum extruded tubes with different cross-sectional shapes, Materials and Design, Vol. 20, 41-49, 1999.

24. Peroni, L., Avalle, M., Petrella, V., Monacelli, G., Strain-rate effects on the energy absorption capacity of crash boxes with different geometry, Structures Under Shock and Impact VII, N. Jones, Brebbia, C. A., and Rajendran A. M. (Editors), WIT Press, Southampton and Boston, pp 259-268, 2002.

25. Tarigopula, V., Langseth, M., Hopperstad, O. S., Clausen, A. H., Axial crushing of thin-walled high-strength steel sections, International Journal of Impact Engineering, Vol. 32, No. 5, 847-882, 2006.

26. Tarigopula, V., Langseth, M., Hopperstad, O. S., Clausen, A. H., An experimental and numerical study of energy absorption in thin-walled high-strength steel sections, Impact loading of Lightweight Structures, Ed., M. Alves, N. Jones, WIT Press, Southampton, U.K., Boston, U.S., WIT Transactions on Engineering Sciences, Vol. 49, pp 495-507, 2005.

27. Karagiozova, D., Jones, N., On dynamic buckling phenomena in axially loaded elastic-plastic cylindrical shells, International Journal of Non-Linear Mechanics, Vol. 37, No. 7, 1223-1238, 2002.

28. Karagiozova, D., Jones, N., Dynamic Buckling of Elastic-Plastic Square Tubes Under Axial Impact. Part II – Structural Response, International Journal of Impact Engineering, Vol. 30, No. 2, 167-192, 2004

29. Seitzberger, M., Rammerstorfer, F. G., Gradinger, R., Degischer, H. P., Blaimschein, M., Walch, C., Experimental studies on the quasi-static axial crushing of steel columns filled with aluminium foam, International Journal of Solids and Structures, Vol. 37, 4125-4147, 2000.

30. Al Galib, D., Limam, A., Experimental and numerical investigation of static and dynamic axial crushing of circular aluminum tubes, Thin-Walled Structures, Vol. 42, 1103-1137, 2004.

31. Karagiozova, D., Jones, N., Influence of stress waves on the dynamic progressive and dynamic plastic buckling of cylindrical shells, International Journal of Solids and Structures, Vol. 38, No. 38/39, 6723-6749, 2001.

32. Birch, R. S., Jones, N., Dynamic and Static Axial Crushing of Axially Stiffened Cylindrical Shells, Journal of Thin Walled Structures, Vol. 9, 29-60, 1990.

33. Jones, N., Papageorgiou, E. A., Dynamic Axial Plastic Buckling of Stringer Stiffened Cylindrical Shells, International Journal of Mechanical Sciences, Vol. 24, No.1, 1-20, 1982.

34. Jones, N., Birch, R. S., Dynamic and Static Axial Crushing of Axially Stiffened Square Tubes, proceedings of Institution of Mechanical Engineers, Vol. 204C, 293-310, 1990.

35. Paik, J. K., Chung, J. K., Chun, M. S., On quasi-static crushing of a stiffened square tube, Journal of Ship Research, Vol. 40, No. 3, 258-267, 1996.

36. Paik, J. K., Wierzbicki, T., A benchmark study on crushing and cutting of plated structures, Journal of Ship Research, Vol. 41, No. 2, 147-160, 1997.

37. Adachi, T., Tomiyama, A., Araki, W., Yamaji, A., Energy absorption of a thin-walled cylinder with ribs subjected to axial impact, International Journal of Impact Engineering, Vol. 35, No. 2, 65-79, 2008.

38. Chen, W., Wierzbicki, T., Relative merits of single-cell, multi-cell and foam-filled thin-walled structures in energy absorption, Thin-Walled Structures, Vol. 39, 287-306, 2001.

39. Zhang, A., Suzuki, K., A study on the effect of stiffeners on quasi-static crushing of stiffened square tube with non-linear finite element method, International Journal of Impact Engineering, Vol. 34, No. 3, 544-555, 2007.

40. Zhang, X., Cheng, G., A comparative study of energy absorption characteristics of foam-filled and multi-cell square columns, International Journal of Impact Engineering, Vol. 34, No.11, 1739-1752, 2007.

41. Hou, S., Li, Q., Long, S., Yang, X., Li, W., Multiobjective optimisation of multi-cell sections for the crashworthiness design, International Journal of Impact Engineering, Vol. 35, No. 11, 1355-1367, 2008.

42. Hanssen, A. G., Langseth, M., Hopperstad, O. S., Static and dynamic crushing of square aluminium extrusions with aluminium foam filler, International Journal of Impact Engineering, Vol. 24, No. 4, 347-383, 2000.

43. Hanssen, A. G., Langseth, M., Hopperstad, O. S., Static and dynamic crushing of circular aluminium extrusions with aluminium foam filler, International Journal of Impact Engineering, Vol. 24, No. 5, 475-507, 2000.

44. Santosa, S P, Wierzbicki, T., Hanssen, A G., Langseth, M., Experimental and numerical studies of foam-filled sections, International Journal of Impact Engineering, Vol. 24, No. 5, 509-534, 2000.

45. Lu, G., Yu, T. X., Energy absorption of structures and materials, CRC Press, New York, Woodhead Publishing Limited, Cambridge, UK, 2003.

46. Karagiozova, D., Alves, M., Jones, N., Inertia Effects in Axisymmetrically Deformed Cylindrical Shells Under Axial Impact, International Journal of Impact Engineering, Vol. 24, No. 10, 1083-1115, 2000

47. Abramowicz, W., Jones, N., Transition from Initial Global Bending to Progressive Buckling of Tubes Loaded Statically and Dynamically, International Journal of Impact Engineering, Vol. 19, No. 5/6, 415-437, 1997.

48. Karagiozova, D., On the dynamic collapse of circular and square tubes under axial impact, Advances in Dynamics and Impact Mechanics, Edited C. A. Brebbia, and G. N. Nurick, WIT Press, Southampton and Boston, pp 1-22, 2003.

Specimen number	N	T/C	δ_e / L	ψ
US-2	0	0	0.760	0.574
LS-7	4	0.15	0.664	0.578
LS-1	4	0.20	0.633	0.638
LS-2	4	0.30	0.687	0.795

TABLE 1

Static energy-absorbing effectiveness factors for the axial crushing of square tubes with four external stiffeners [35].

	H = 1mm	H = 1mm	H = 2mm	H =2mm
	empty	with foam	empty	with foam
square tube	0.69	2.47	1.10	2.07
double-cell	0.87	2.89	1.23	2.33
triple-cell	0.95	3.01	1.35	2.45

TABLE 2

Static energy-absorbing effectiveness factors for the axial crushing of empty and foam-filled single-cell, double-cell and triple-cell square tubes having C = 80 mm, σ_f = 3.1 MPa, σ_o =161.7 MPa, ε_r = 0.19 and δ_e/L = 0.75.

FIGURE TITLES

Figure 1. Circular cylindrical shells crushed axially with G = 102kg and V_o = 13.28 m/s [11,12]. o : aluminium alloy 6063T6; x : mild steel; □: stainless steel 304. σ_o is the mean flow stress.

Figure 2. Square tubes crushed with dynamic axial loads.

Experimental results with G = 28 kg and V_o = 8.85 m/s [13]. x^1: mild steel, □: stainless steel. Table 2 of [12] with G < 100 kg and V_o < 17.3 m/s. x^2: mild steel (average) [14], •: aluminium alloy 6060T4 [15], o: aluminium alloy 6060T6 [15], Δ: brass [16].

Figure 3. Square tubes crushed with dynamic axial loads.
Experimental results. Δ: Table 2 of [12] ([5, 10, 14-17]), x: [13], □: [23], o: [24] and ∇: [25,26].

Figure 4. Honeycomb sections crushed with dynamic axial loads.

Experimental results. o: TRIP 600 Steel, Table 5 of Reference [12] ([9, 19, 20]), □ and Δ: aluminium alloy 5052-H38 (σ_o = 272.5 MPa) and 5056-H38 (σ_o = 380 MPa)[18], respectively.

Figure 5. Variation of ψ(o) and ψ'(•) with the cross-sectional shape of mild steel sections [12].

Figure 6. Energy-absorbing effectiveness factors according to equation (6).
Aluminium alloy 6061 tubes with rectangular cross-sections of area A with
V_o = 1.7 m/s and σ_o = 206 MPa [23]. □: "welded" end plates, ■: "unwelded" end plates.
*: the impact energy reported for this test specimen appears to be anomalous.

Figure 7. Energy-absorbing effectiveness factors according to equation (6).
(a) aluminium alloy 6061 circular cylindrical shells with mean diameter-to-thickness ratios (2R/H) and V_o = 1.7 m/s and σ_o = 206 MPa [23].
o : welded; × : unwelded.
(b) aluminium alloy 6061 tubes with rectangular and square cross-sections having mean side length-to mean thickness ratios (C/H) and V_o = 1.7 m/s and σ_o = 206 MPa [23].
o : welded; × : unwelded.
*: the impact energy reported for this test specimen appears to be anomalous.

Figure 8. Energy-absorbing effectiveness factors according to equation (6).
(a) × : square tubes, aluminium alloy 6060 T4, σ_o =114.5 and 126.5 MPa [12, 15,17]. : square tubes, aluminium alloy 6060 T6, σ_o = 198 and 203 MPa [12, 15,17]. o : circular cylindrical tubes, aluminium alloy 6060 T5, σ_o = 241.4 MPa [30].
(b) ◊ : aluminium alloy 5052 H38 honeycomb sections (Type 3), σ_o = 272.5 MPa [18].
♦: aluminium alloy 5056 H38 honeycomb sections (Type 5), σ_o = 380 MPa [18].
Δ: high strength steel DP 800 top-hat sections, σ_o = 665 MPa [25].
▲: high strength steel DP 800 square sections, σ_o = 665 MPa [25].
□: mild steel square sections (series N), σ_o = 372 MPa [13].
■: stainless steel AISI 304 square sections (series A), σ_o = 604 MPa [13].

Figure 9. Energy-absorbing effectiveness factor for axially stiffened (N = 4) and unstiffened mild steel circular cylindrical shells subjected to static and dynamic axial loads versus T/D, where T is the depth of a stiffener and D is the mean diameter of a tube (σ_o = 284.5 MPa, $\delta_e/L = 0.75$) [32].

◊, o, •: static loading for unstiffened and axially stiffened cylindrical shells with four external and four internal stiffeners, respectively.

Δ, ▲: impact loading at $V_o \approx 11.7$ m/s for external and internal stiffeners, respectively.

∇, ▼: impact loading at $V_o \approx 10.6$ m/s for external and internal stiffeners, respectively.

Figure 10. Energy-absorbing effectiveness factor for axially stiffened (N = 4) and unstiffened mild steel square tubes versus T/C, where T is the depth of a stiffener and C is the mean side length of a tube (σ_o = 275.6 MPa, $\delta_e/L = 0.75$) [34].

See the legend of Figure 9 for the notation.

Figure 11. Variation of the dynamic energy-absorbing effectiveness factor, ψ', according to equation (13) with the mean flow stress (σ_o) of aluminium alloy 6060 square tubes filled with aluminium foam having a nominal density ρ_f [42].

o: experimental values [42]. •: specimen has possibly bottomed-out.

Figure 12. Variation of the dynamic energy-absorbing effectiveness factor, ψ', according to equation (13) with the mean flow stress (σ_o) of aluminium alloy 6060 T4 circular tubes filled with aluminium foam having a nominal density ρ_f [43].

o: experimental results for H = 1.40 - 1.42mm. Δ: experimental results for H = 1.97 - 2.01mm. □: experimental results for H = 2.35 - 2.46mm.

Figure 13. (a) Single-cell, (b) double-cell and (c) triple-cell cross-sections of square tubes crushed axially. All parts of the cross-sections have a uniform thickness H.

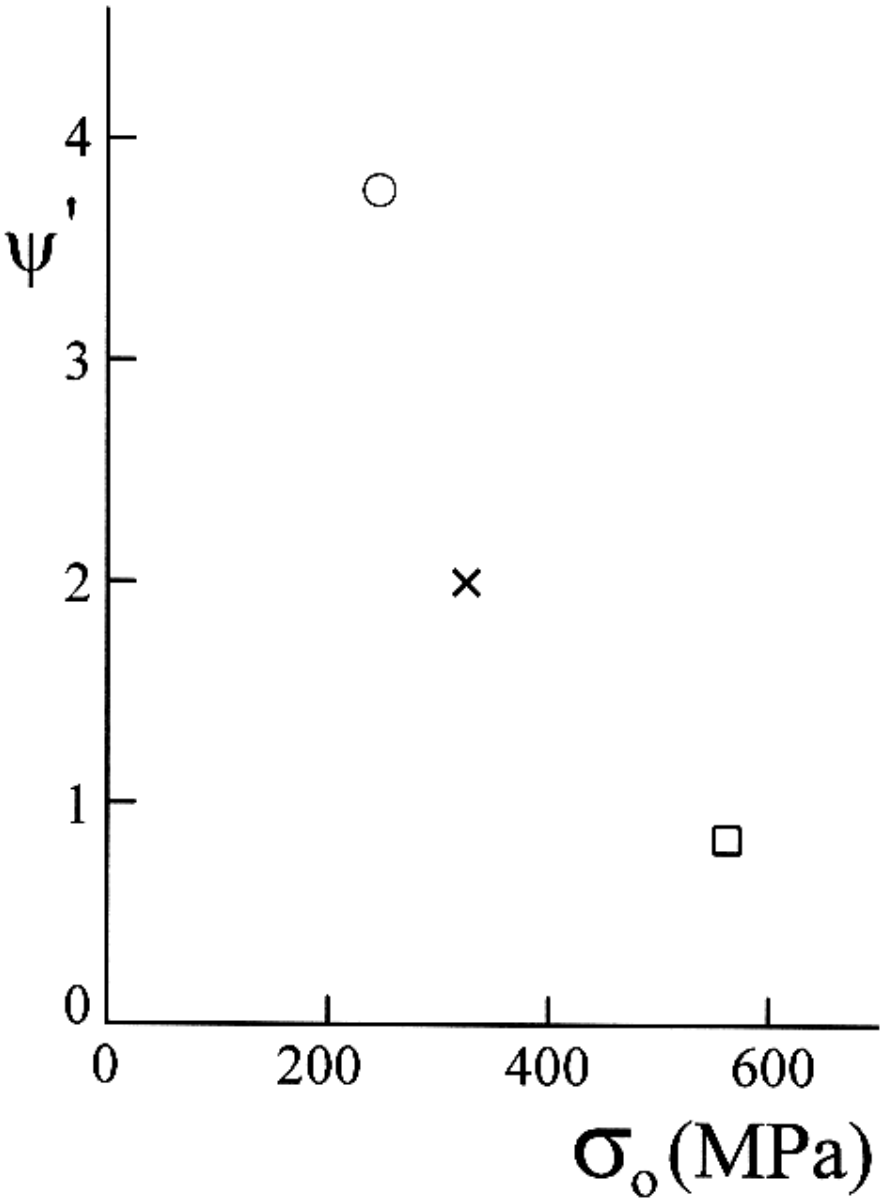

Fig.1

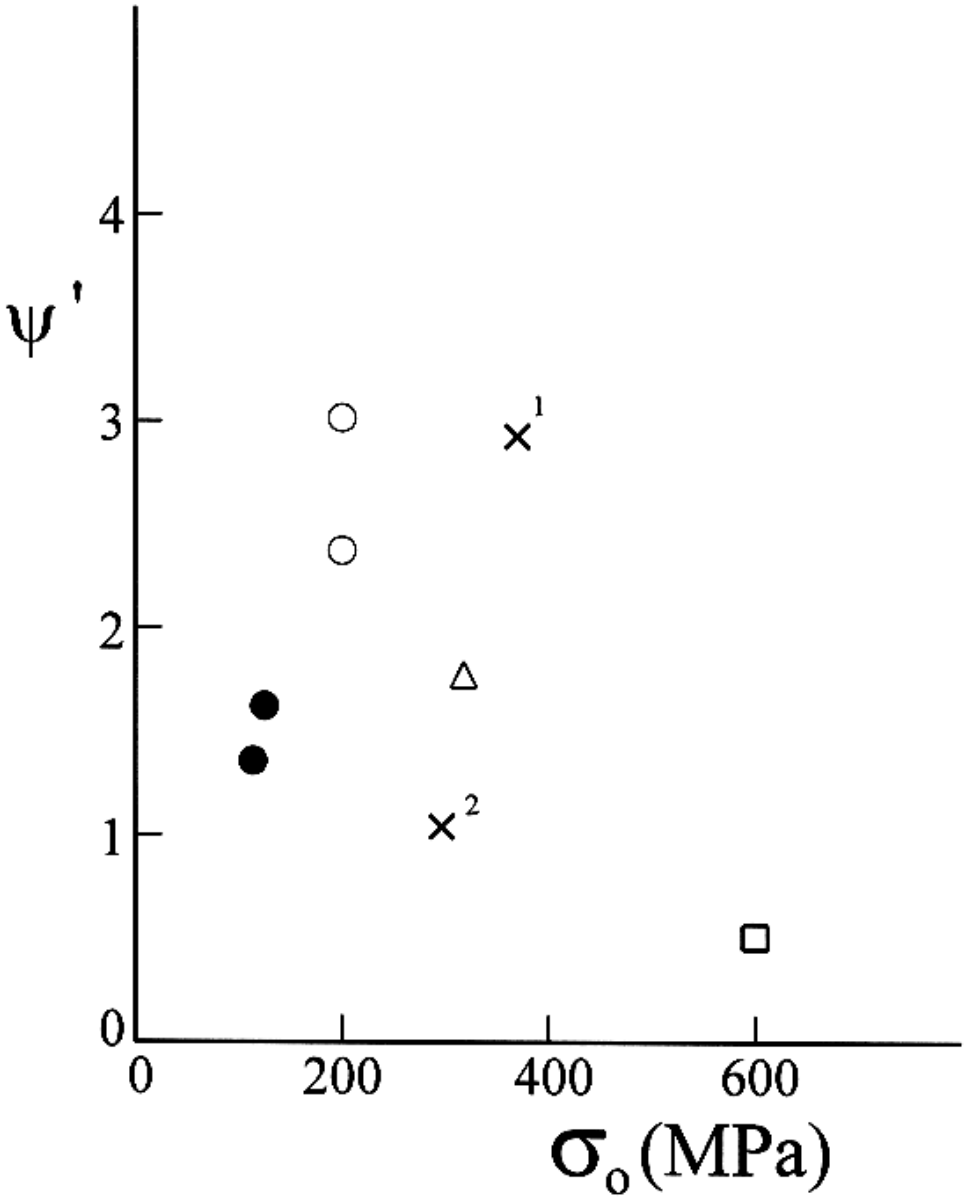

Fig.2

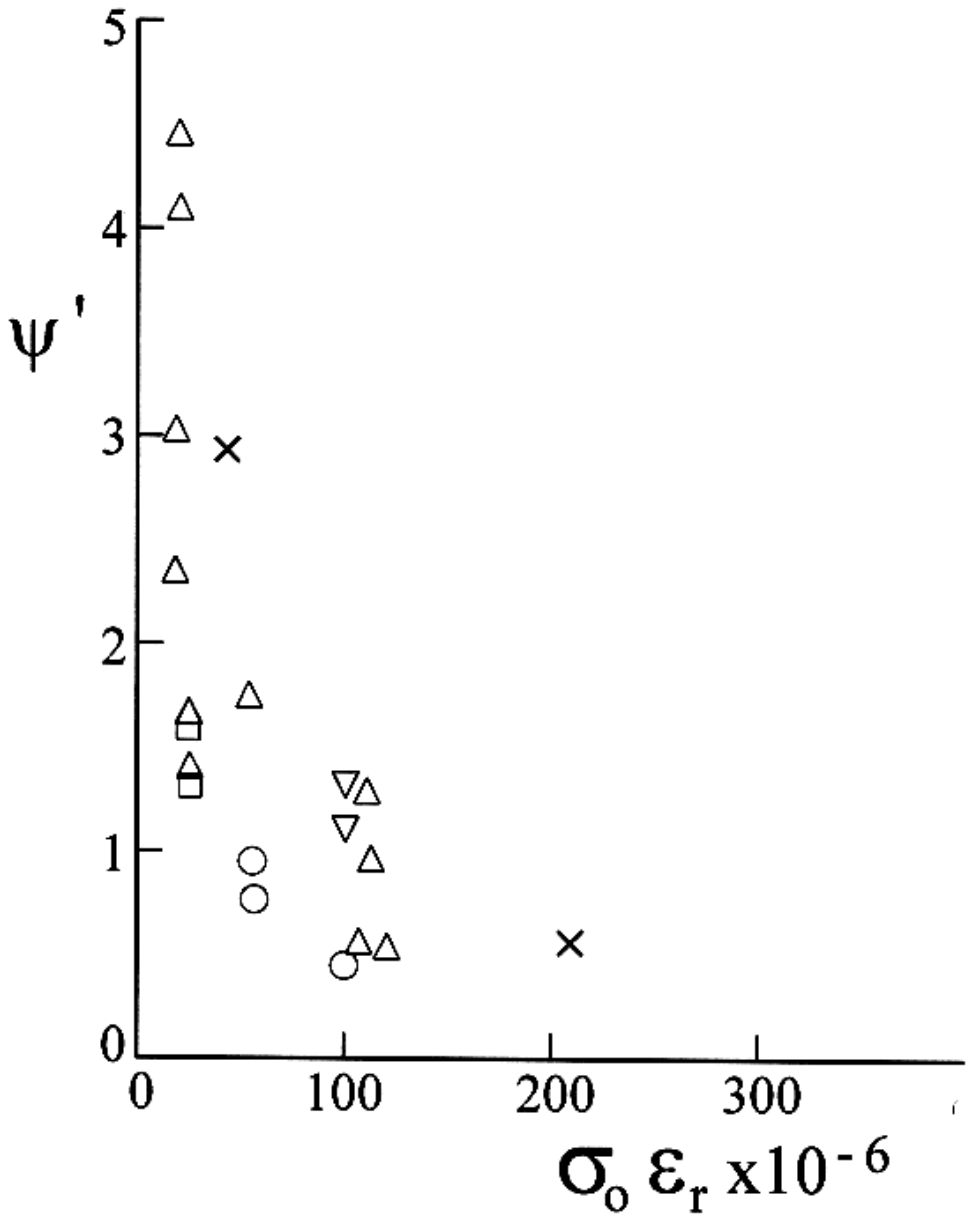

Fig.3

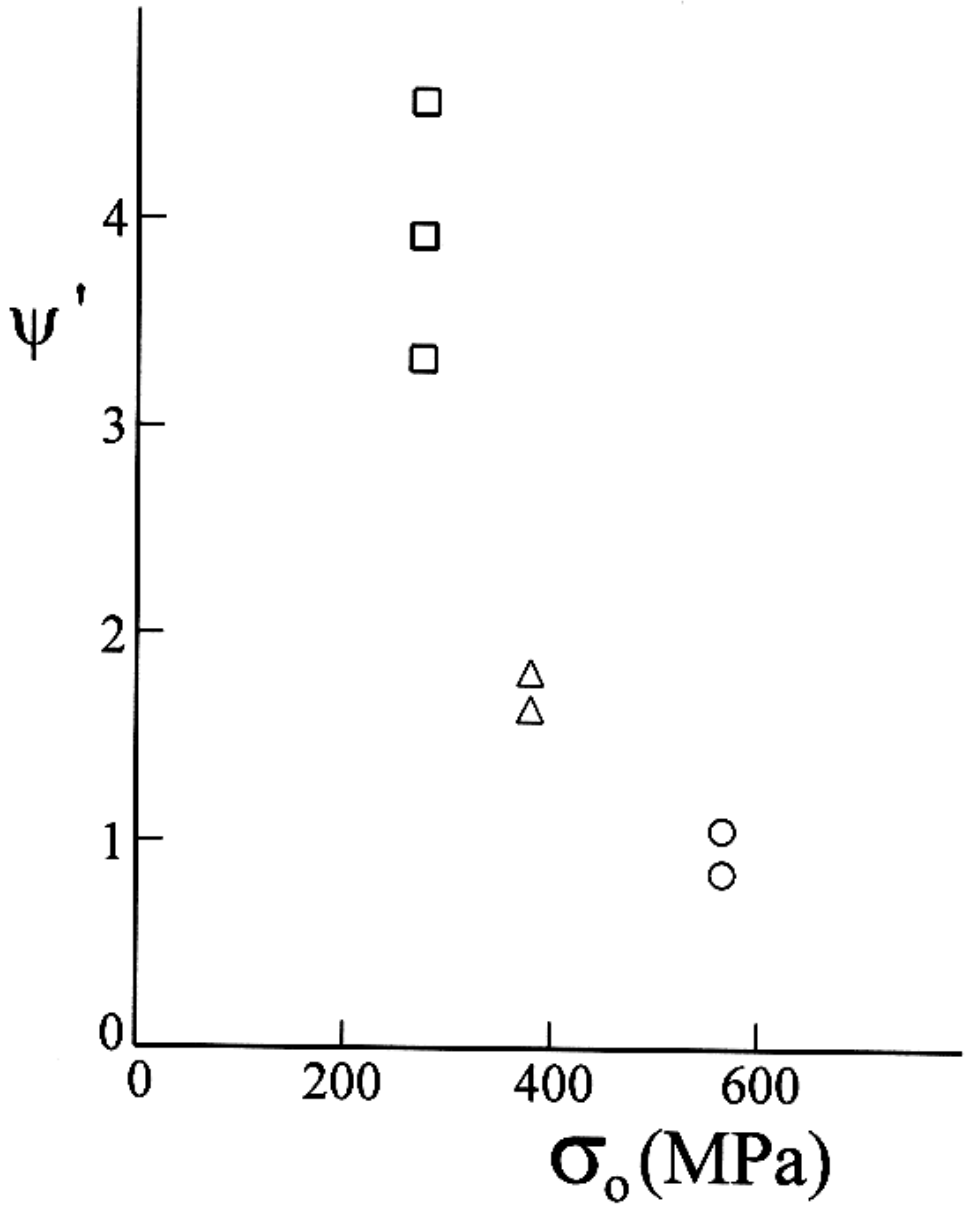

Fig. 4

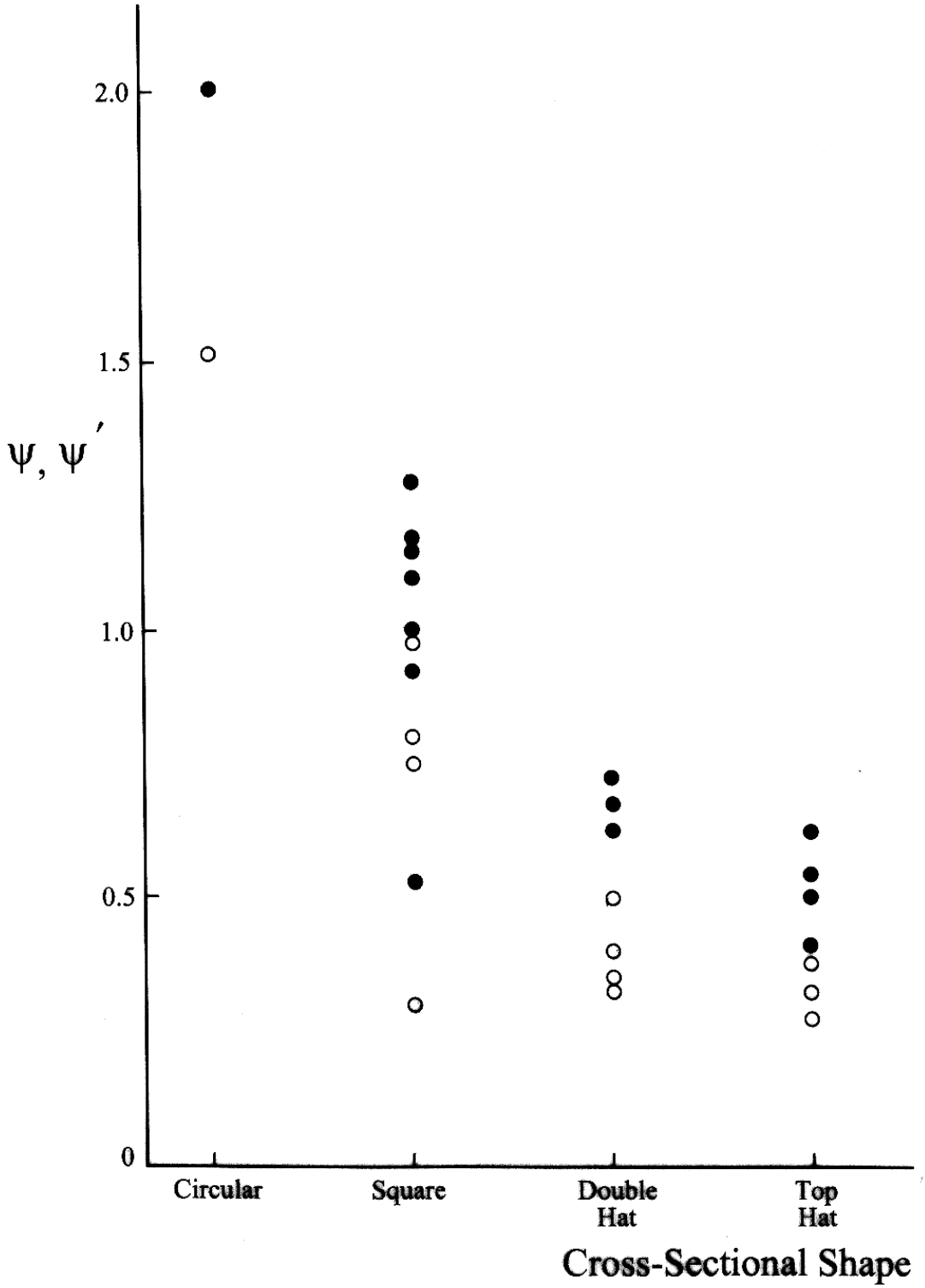
2.0
1.5
1.0
0.5
0
ψ, ψ′
Circular
Square
Double Hat
Top Hat
Cross-Sectional Shape

Fig.5

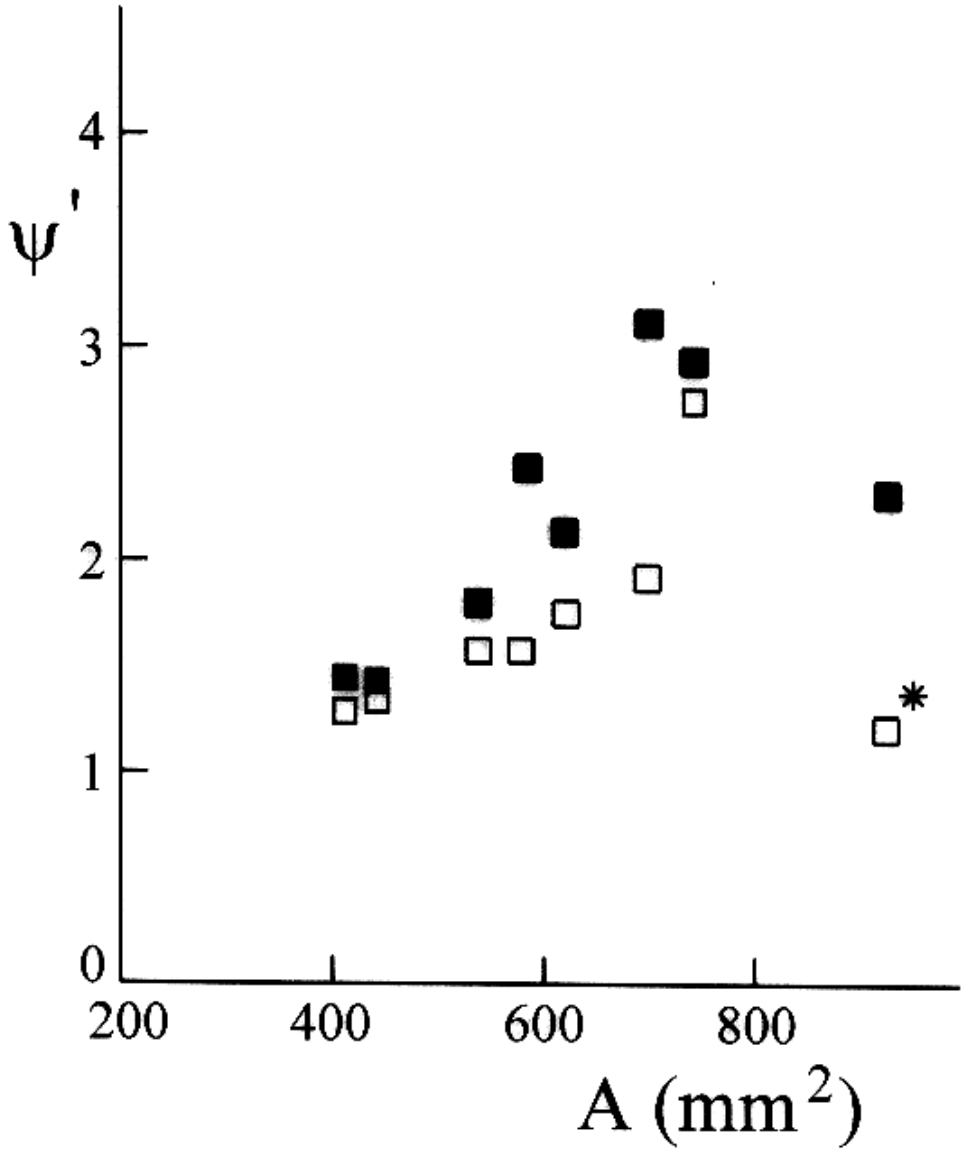

Fig.6

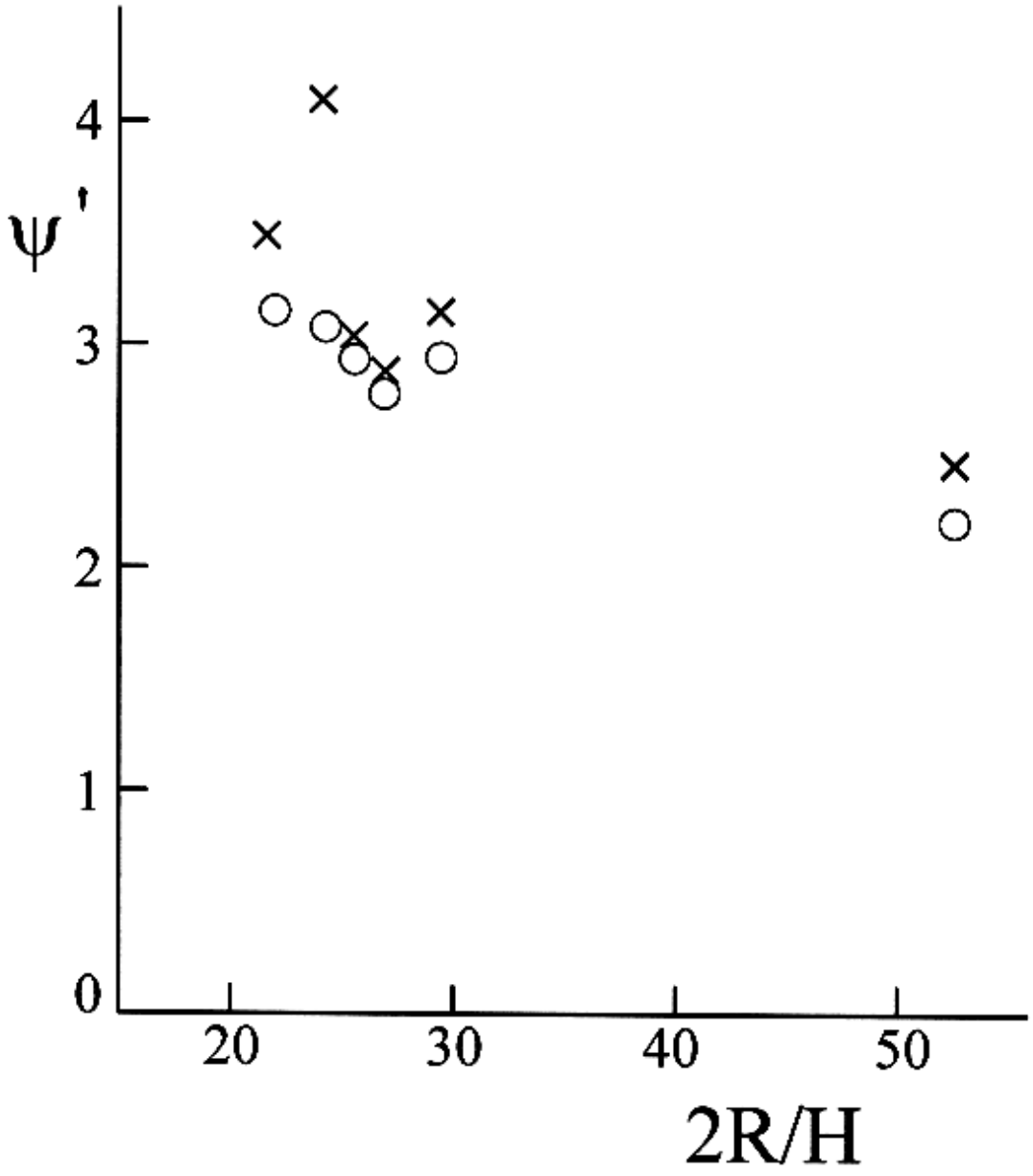

Fig. 7 (a)

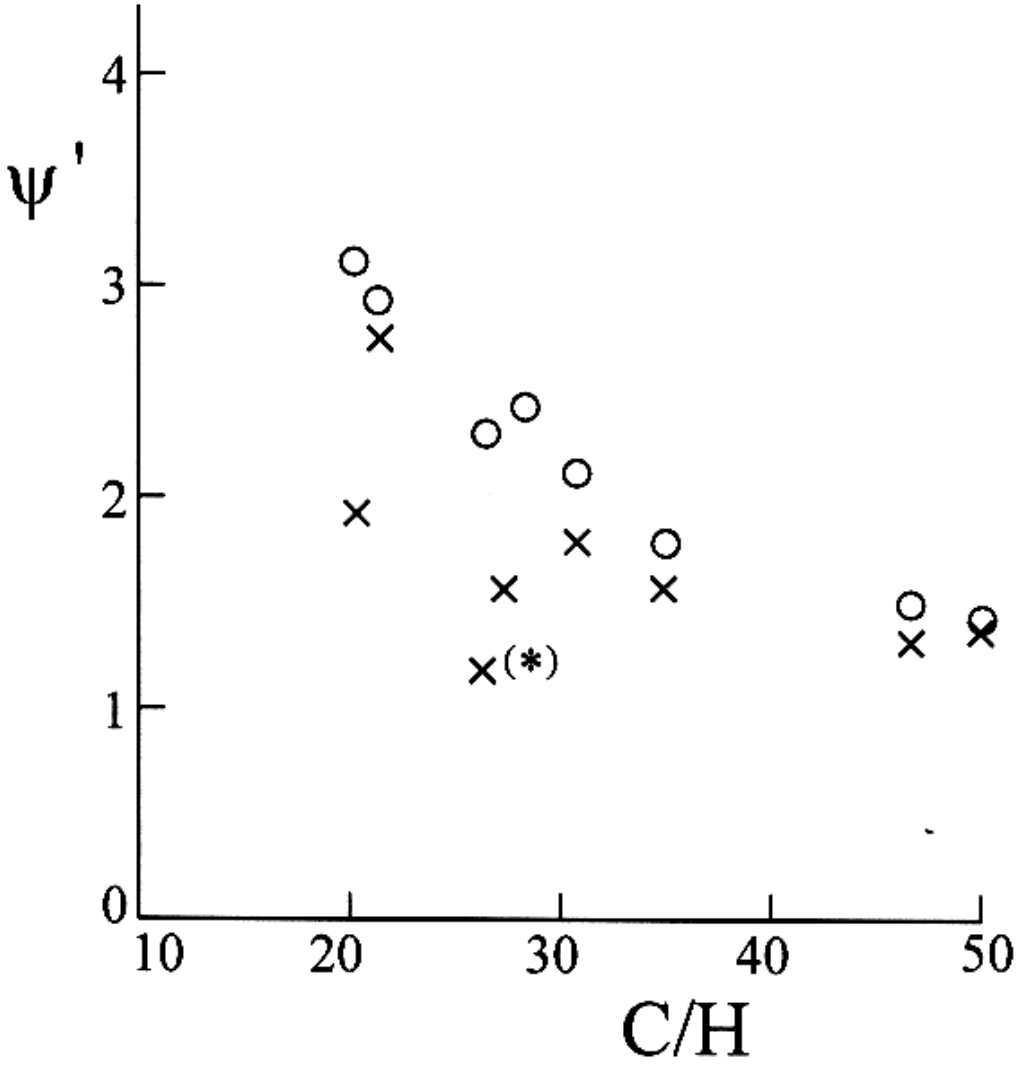

Fig. 7(b)

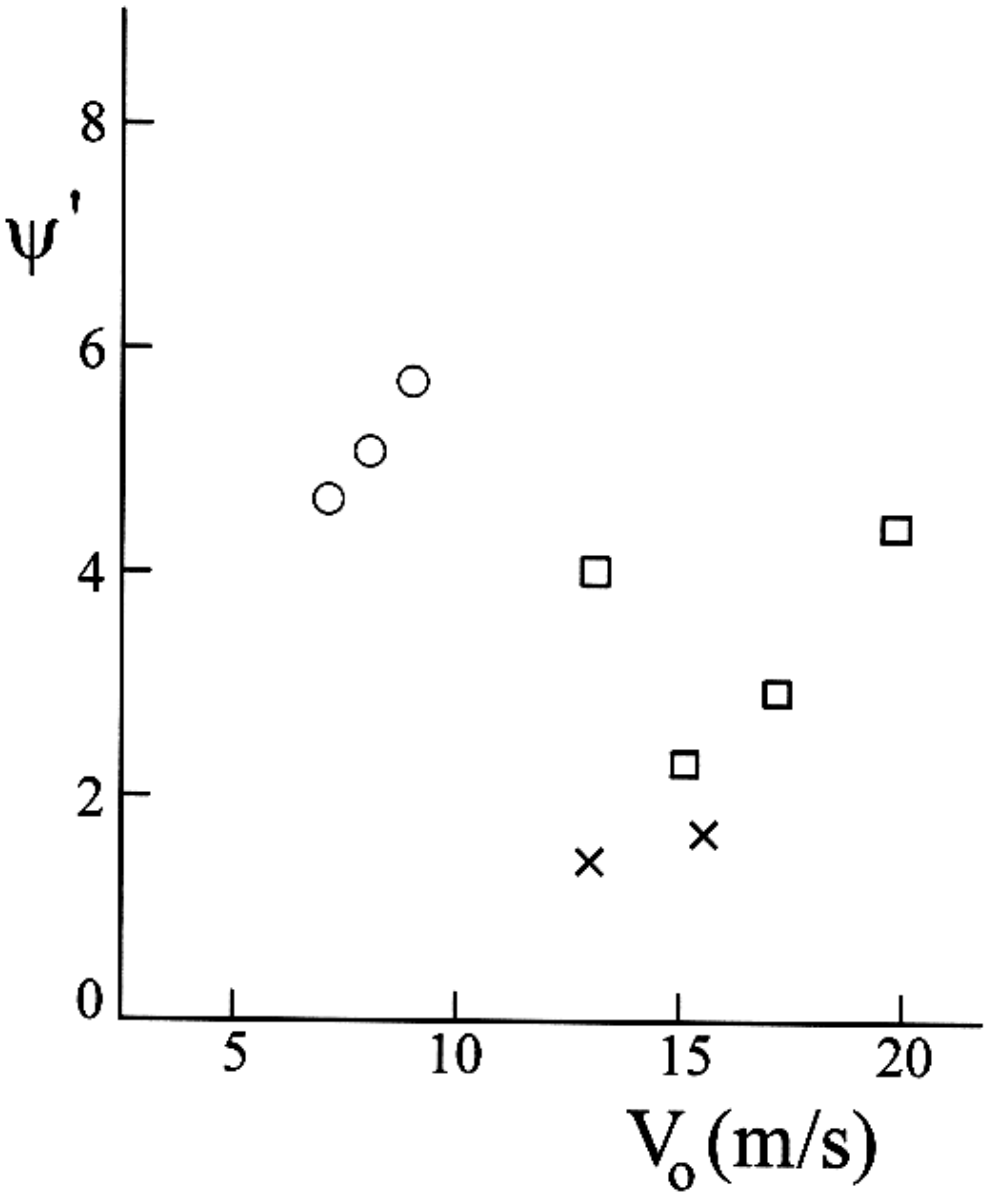

Fig.8(a)

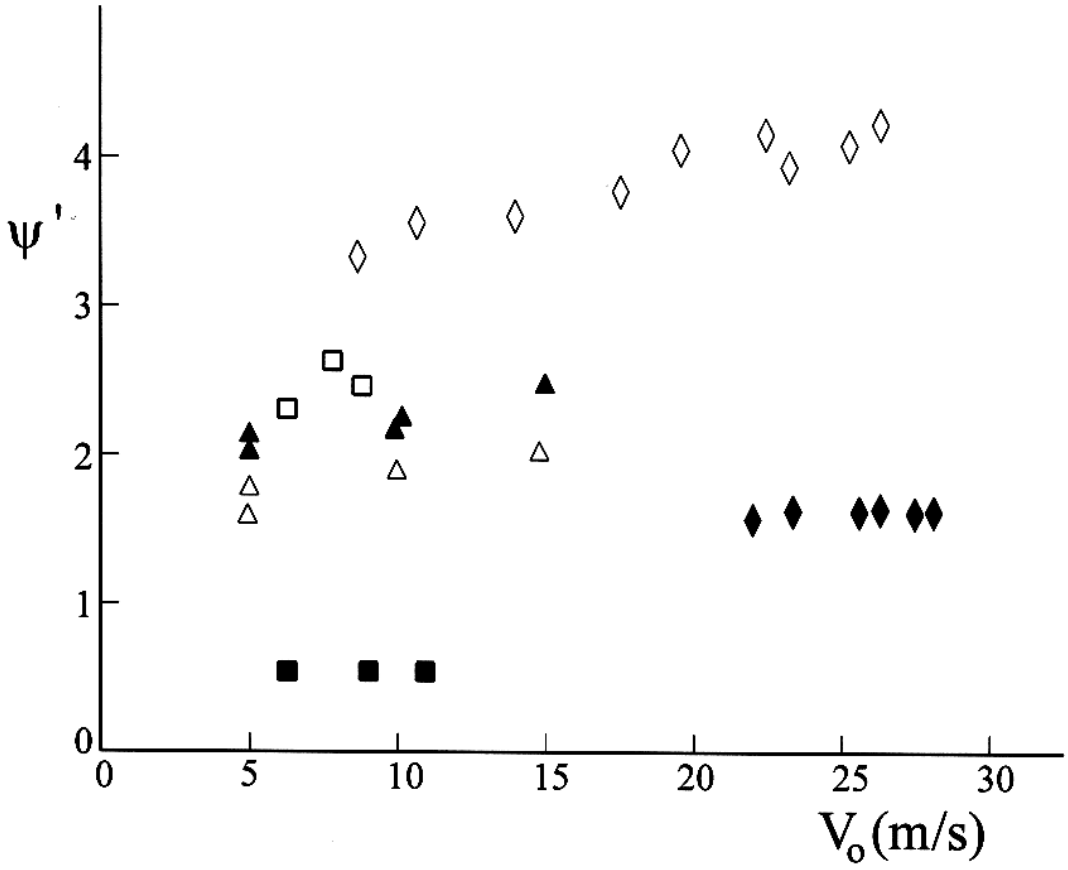

Fig. 8(b)

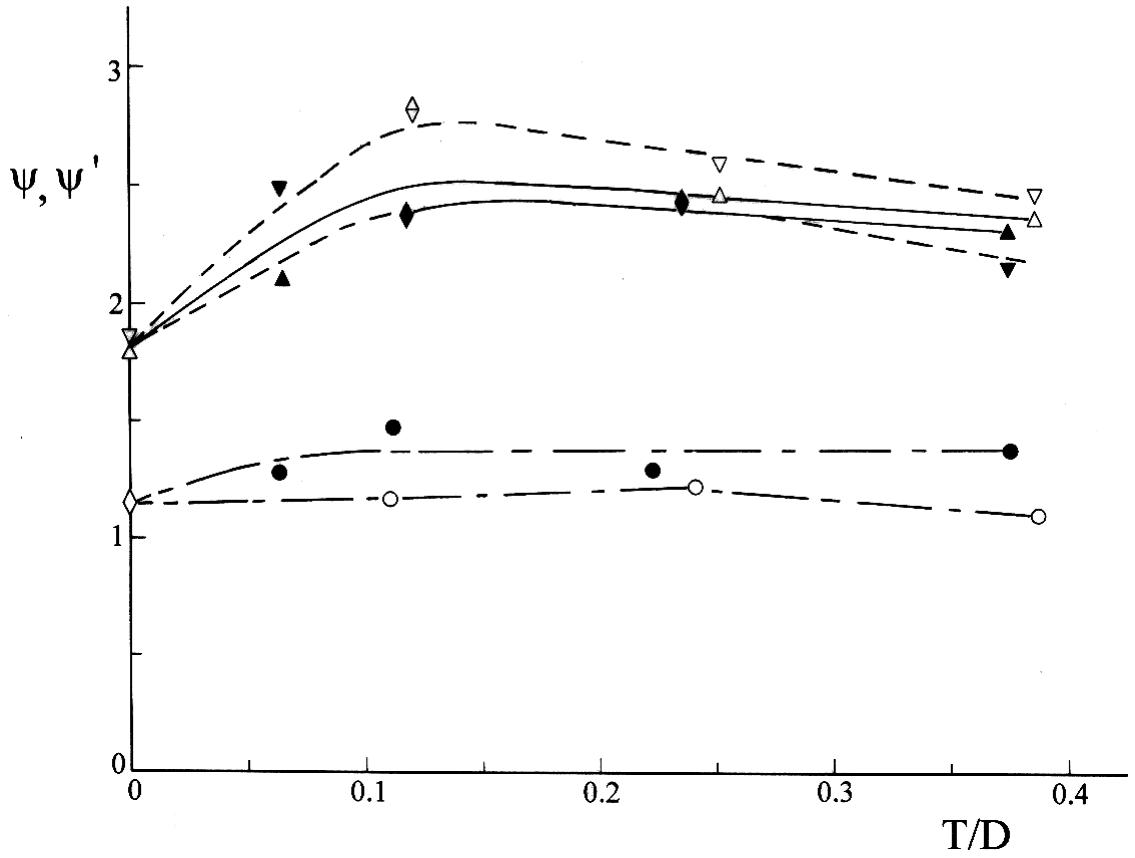

Fig. 9

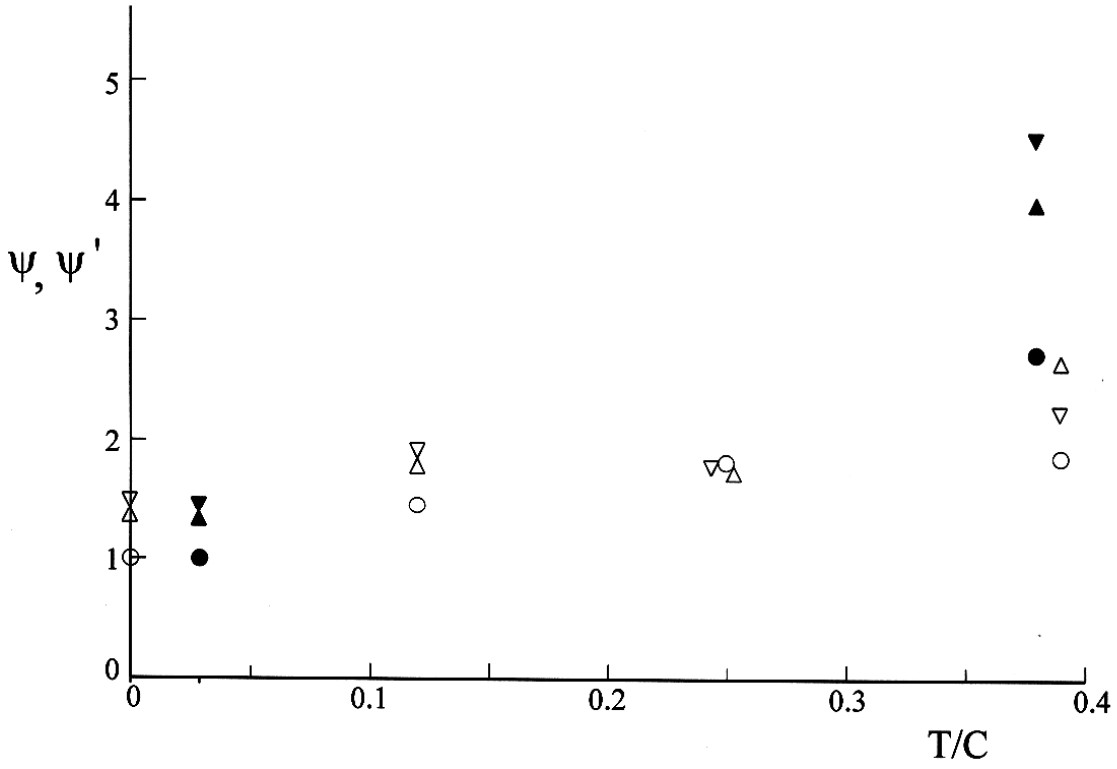

Fig. 10

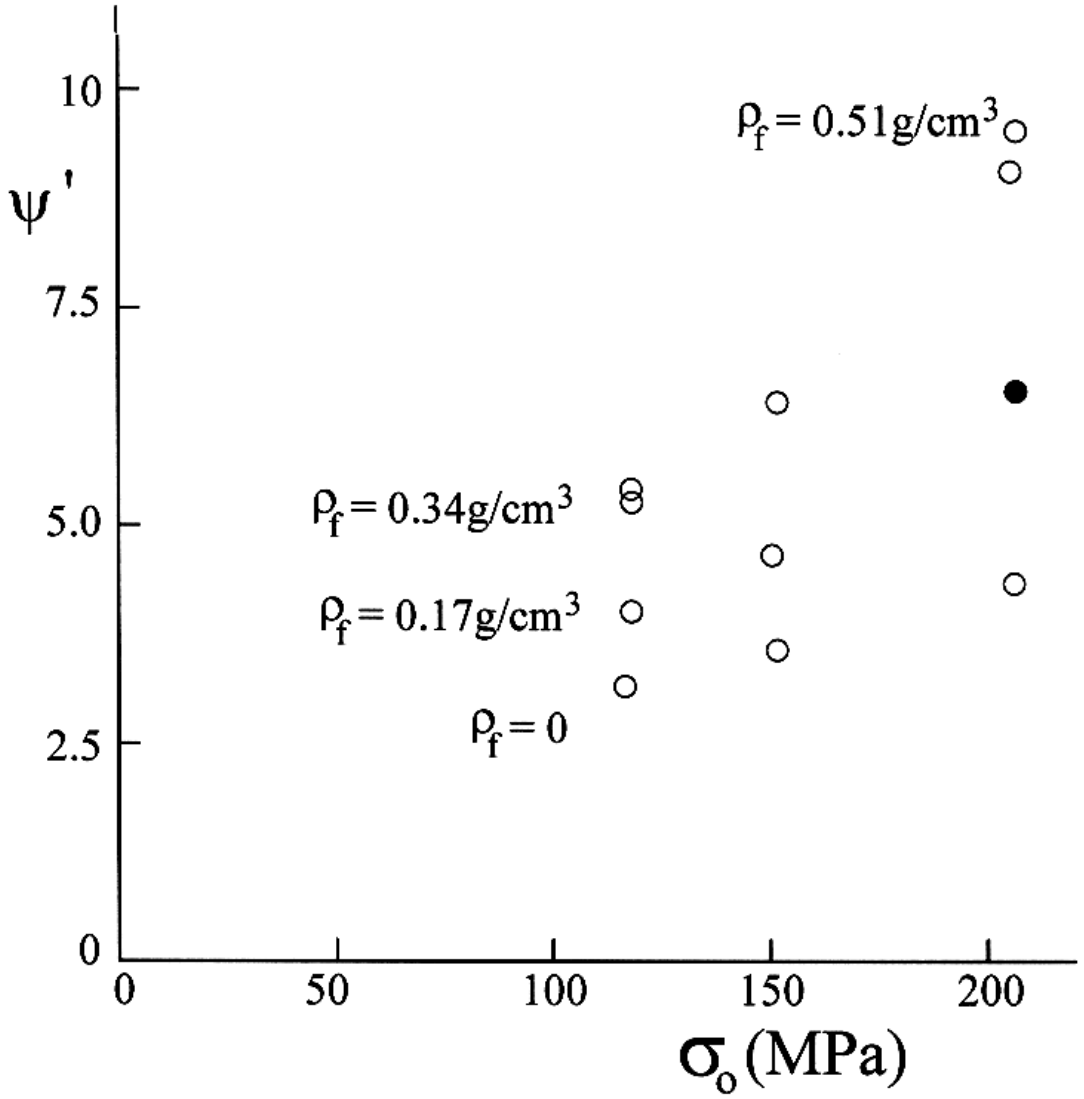
10
7.5
5.0
2.5
0
ψ '
0
50
100
150
200
σo (MPa)
ρf = 0.51g/cm3
ρf = 0.34g/cm3
ρf = 0.17g/cm3
ρf = 0

Fig. 11

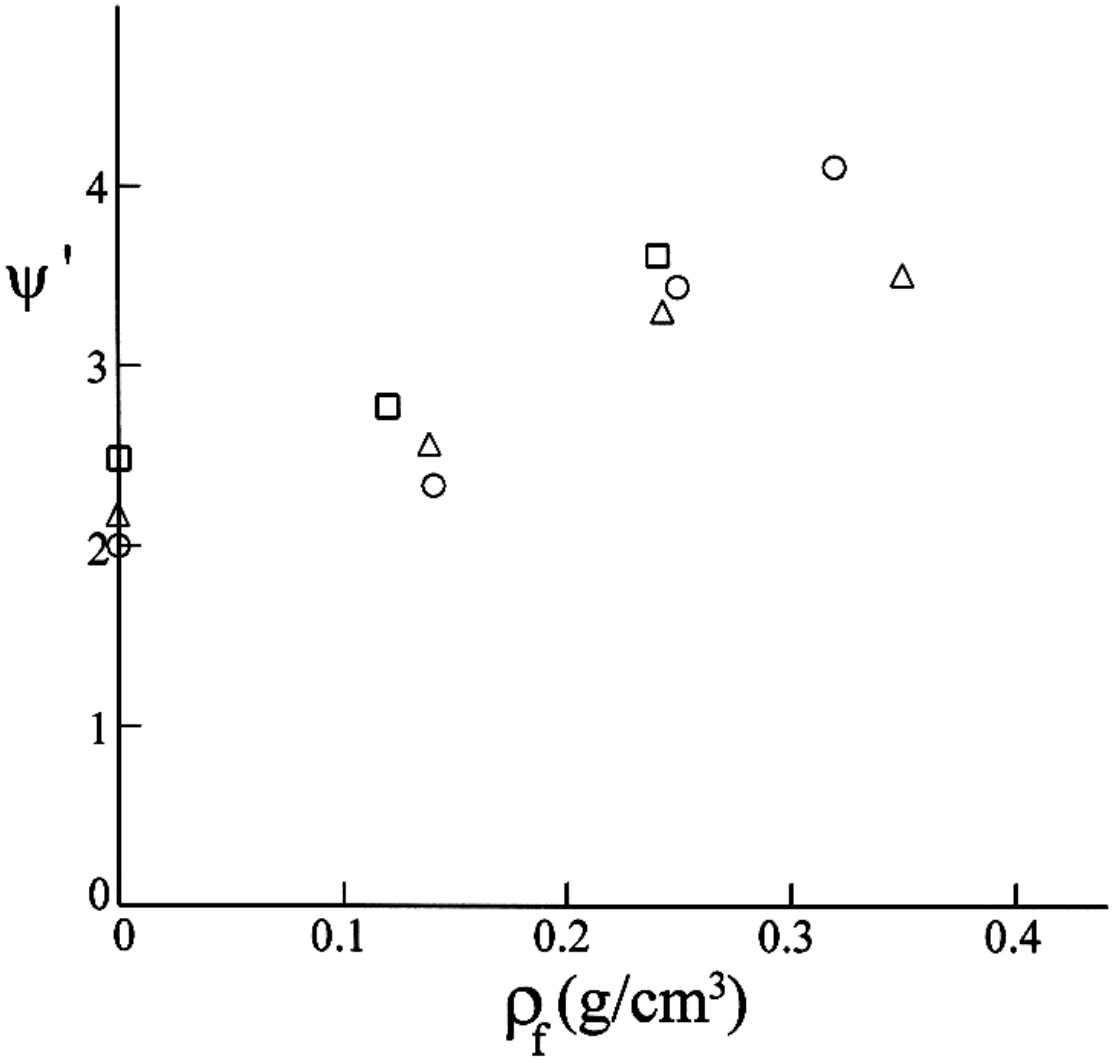

Fig. 12

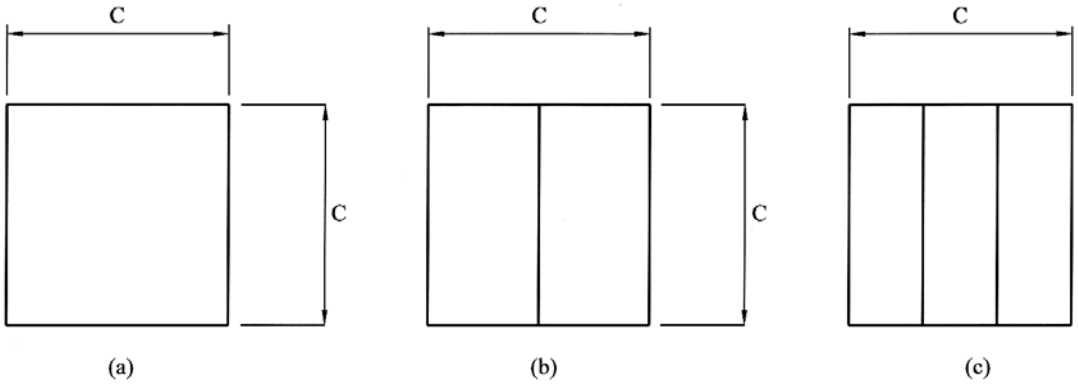

Fig.13